

Published in final edited form as:

Neuroimage. 2018 October 01; 179: 11–29. doi:10.1016/j.neuroimage.2018.06.018.

Construction of a Neonatal Cortical Surface Atlas Using Multimodal Surface Matching in the Developing Human Connectome Project

Jelena Bozek^{a,1}, Antonios Makropoulos^b, Andreas Schuh^b, Sean Fitzgibbon^c, Robert Wright^d, Matthew F. Glasser^{e,f}, Timothy S. Coalson^e, Jonathan O’Muircheartaigh^{d,h}, Jana Hutter^d, Anthony N. Price^d, Lucilio Cordero-Grande^d, Rui Pedro A. G. Teixeira^d, Emer Hughes^d, Nora Tusor^d, Kelly Pegoretti Baruteau^d, Mary A. Rutherford^d, A David Edwards^d, Joseph V. Hajnal^d, Stephen M. Smith^c, Daniel Rueckert^b, Mark Jenkinson^c, Emma C. Robinson^g

^aFaculty of Electrical Engineering and Computing, University of Zagreb, Zagreb, Croatia

^bBiomedical Image Analysis Group, Department of Computing, Imperial College London, London, UK

^cWellcome Centre for Integrative Neuroimaging, FMRIB, Nuffield Department of Clinical Neurosciences, University of Oxford, Oxford, UK

^dCentre for the Developing Brain, Division of Imaging Sciences and Biomedical Engineering, King’s College London, London, UK

^eDepartment of Neuroscience, Washington University School of Medicine, St. Louis, MO, USA

^fSt. Lukes Hospital, St. Louis, MO, USA

^gDepartment of Biomedical Engineering, School of Biomedical Engineering and Imaging Sciences, Kings College London, London, UK

^hDepartment of Neuroimaging, Institute of Psychiatry, Psychology and Neuroscience, Kings College London, London, UK

Abstract

We propose a method for constructing a spatio-temporal cortical surface atlas of neonatal brains aged between 36 and 44 weeks of post-menstrual age (PMA) at the time of scan. The data were acquired as part of the Developing Human Connectome Project (dHCP), and the constructed surface atlases are publicly available. The method is based on a spherical registration approach: Multimodal Surface Matching (MSM), using cortical folding for driving the alignment. Templates have been generated for the anatomical cortical surface and for the cortical feature maps: sulcal depth, curvature, thickness, T1w/T2w myelin maps and cortical regions. To achieve this, cortical surfaces from 270 infants were first projected onto the sphere. Templates were then generated in two stages: first, a reference space was initialised via affine alignment to a group average adult template. Following this, templates were iteratively refined through repeated alignment of

*Corresponding author: jelena.bozek@fer.hr (Jelena Bozek).

individuals to the template space until the variability of the average feature sets converged. Finally, bias towards the adult reference was removed by applying the inverse of the average affine transformations on the template and de-drifting the template. We used temporal adaptive kernel regression to produce age-dependant atlases for 9 weeks (36 to 44 weeks PMA). The generated templates capture expected patterns of cortical development including an increase in gyrification as well as an increase in thickness and T1w/T2w myelination with increasing age.

Keywords

cortical surface atlas; MSM; neonatal; MRI; dHCP

1 Introduction

During the third trimester, the developing brain undergoes significant increases in size and gyrification. At birth, all primary and secondary folding features of the human cerebral cortex have been well established (Hill et al., 2010), and spatially consistent distributions of major sulci can be observed across individuals (Meng et al., 2014). Understanding the mechanisms of these processes, and the characteristics of normal growth, is important for detecting possible abnormalities that could lead to neurodevelopmental disorders.

Improvements in brain imaging techniques have resulted in the increase of neonatal brain MR studies and the availability of high quality neonatal brain MR images. One such study is the Developing Human Connectome Project¹ (dHCP) led by King's College London, Imperial College London, and Oxford University. The goal of the project is to acquire and analyse structural, functional and diffusion Magnetic Resonance (MR) images of the brain from fetuses and neonates, in order to generate the first spatio-temporal connectome of early life. So far, the acquired dataset consists mainly of neonatal MR images, and thus we will focus on the neonatal cortical surface atlas construction in this paper.

Analysing and visualising the functional and structural changes in the cortex requires a framework for comparing cortical anatomy and brain functional activations across subjects. This can be achieved through the development of common template spaces (or atlases). However, it is challenging to construct fetal and neonatal volumetric, as well as cortical surface, atlases due to the rapid development of cortical anatomies over time. Several volumetric neonatal atlases have been constructed (e.g. Kuklisova-Murgasova et al. (2011); Serag et al. (2012); Makropoulos et al. (2016)). Of these, Kuklisova-Murgasova et al. (2011) constructed a 4D probabilistic volumetric atlas using rigid and affine registrations, and kernel regression; and Serag et al. (2012) built a spatio-temporal volumetric atlas using pairwise registrations, performed using volumetric Free-Form Deformations (FFDs) (Rueckert et al., 1999), where the resulting transformations were averaged using adaptive kernel regression. Using registrations among all subject pairs they eliminated bias towards any of the subjects. Makropoulos et al. (2016) built a spatio-temporal structural atlas of the

¹<http://www.developingconnectome.org>

brain for 82 cortical and subcortical structures based on an automatic segmentation algorithm for parcellating the neonatal brain.

However, volumetric atlases are limited in that they allow only volume-based analysis and are designed mostly for the analysis of subcortical structures, while cortical surface atlases allow the analysis of highly-convoluted and highly-variable cerebral cortex (Van Essen and Dierker, 2007). Furthermore, cortical surface atlases provide a reference space for surface morphometry and subsequent surface-based connectivity analysis in the developing brain (Wright et al., 2015). Another limitation of volumetric atlases is that volumetric registration is not well suited to aligning the cerebral cortical sheet, because in 3D it is necessary to align both the sheet itself and areas within the sheet, whereas in 2D it is necessary only to align areas within the sheet, a much simpler and better conditioned problem in the context of variable folding patterns (Fischl et al., 2008; Glasser et al., 2013, 2016b).

As far as we know, only one term-age neonatal cortical surface atlas has been developed so far. This was constructed by Hill et al. (2010) using landmark-constrained surface registration of 12 term-born neonates (mean gestational age of 39 weeks). For this, six landmarks were delineated on each hemisphere for each subject. These were averaged across subjects and projected onto a standard sphere, used as a template. However, related atlases have been created by Li et al. (2015), who constructed a 4D cortical surface atlas of developing cortex in older infants, with seven time points starting at 1 month until 24 months of age; they used Spherical Demons (Yeo et al., 2010) within a diffeomorphic groupwise registration method. Also, Wright et al. (2015) used spectral surface matching (Lombaert et al., 2013) for constructing a spatio-temporal cortical surface atlas of the developing fetal cortex for each week of gestation from 23 to 37 weeks (total of 15 templates).

The aforementioned atlases are either constructed for one specific target age (Hill et al., 2010) or do not include neonatal data at the term age (Li et al., 2015; Wright et al., 2015). For this reason, we construct an unbiased, spatio-temporal, neonatal cortical surface atlas from age-matched groups of surfaces for each week of term gestation (9 templates in total, from 36 to 44 weeks). Group average maps for cortical folding (sulcal depth and curvature), thickness, myelination (Glasser and Van Essen, 2011), and regional labels (Makropoulos et al., 2014) (Fig 2) have been generated, and per region evaluation of developmental trends have been explored.

The atlas is constructed using Multimodal Surface Matching (MSM) (Robinson et al., 2014, 2018), which is a spherical registration approach that allows flexible alignment of a wide variety of different types of features on the cortical surface, such as cortical folding and myelination. The versatility of MSM originates from using a modular discrete optimisation scheme that allows flexible choice of a similarity measure and is relatively insensitive to local minima. For the neonatal template construction we use a new and improved MSM that allows greater control over the smoothness of the deformations (Robinson et al., 2018). This was used in (Glasser et al., 2016a) to align 449 adult, multi-modal data sets, to a group average template, during development of the Human Connectome Project's (HCP) multi-modal parcellation of the human cerebral cortex. It has the advantage of generating smooth

distortions and improved alignment, especially in areas of significant feature variance attributable to population variability.

In this paper, neonatal templates are generated in a two stage-process. First, an unbiased volumetric reference space is initialised via affine alignment to a group average adult template Conte69 (FS LR, Van Essen et al. (2012), used by the HCP), which resolves differences in the orientation of the subjects. This is left-right symmetric, and allows direct comparison between neonatal and adult feature sets as well as down-stream comparisons between the HCP healthy adult, baby connectome and life-span projects ². The bias towards the adult reference was removed by removing mean scaling from the final template. Following initialisation, the surface templates are iteratively refined, through alignment of fine-scale cortical folding patterns, to generate sharp, unbiased (and anatomically representative) templates for cortical surface analysis and visualisation.

Iterative refinement is commonly used in atlas construction. Evans et al. (1993) used iterative registration to build adult standard volumetric MNI (Montreal Neurological Institute) space. They used a two-stage procedure to construct a template brain that was approximately matched to the Talairach atlas. Guimond et al. (2000) built an average intensity, average shape template of their image set in an iterative manner, using the result of the previous iteration as the reference image. Their average brain models did not evolve significantly after the first iteration. Iterative refinement procedures are also commonly used in the building of adult cortical surface templates Fischl et al. (1999b); Lyttelton et al. (2007).

The results presented here extend the work presented in Bozek et al. (2016), in which a preliminary proof of concept of the proposed method for building an unbiased neonatal cortical surface atlas for 38 to 42 weeks PMA (Post Menstrual Age) was described. In this paper we extend our previous work by including data from a wider range of ages, by using more datasets per week, and by using temporal kernel regression with the adaptive kernel width for averaging to overcome the variation in the distribution of subjects at different ages. Note, in this paper we move away from the computationally expensive, and not easily expandable, pairwise initialisation proposed in Bozek et al. (2016) in favour of affine alignment to an adult atlas. Further, we perform atlas refinement and add another cortical feature, namely cortical thickness. Finally, we perform the analysis of feature maps for left and right hemisphere within different cortical regions as well as computing gyrification index.

In the next section 2 we provide an overview of the dataset (2.1), details on adaptive kernel regression 2.2, used features (2.3), and methods used to generate the atlas (2.4). In section 3 we present the generated cortical surface templates as well as the analysis of the obtained averaged cortical features for left and right hemispheres. Registration code used for generating atlas is available (https://github.com/ecr05/MSM_HOCR) and the atlases constructed from the dHCP cohort are publicly available for download from <http://brain-development.org/brain-atlases/cortical-surface-atlas>.

²<https://www.humanconnectome.org>

2 Methods

2.1 Dataset

MR images were acquired as a part of the Developing Human Connectome Project; this study was approved by the National Research Ethics Committee and informed written consent given by the parents of all participants. Images were obtained from 270 infants with a 3T scanner (Philips) sited inside the Evelina London Children's Hospital Neonatal Intensive Care Unit with full intensive care facilities, using a 32 channel dedicated neonatal head coil (Hughes et al., 2016). Infants were born at a 28-42 (median 39) completed weeks of PMA, and images were obtained 1-80 (median 3) days after birth at 35-44 completed weeks of PMA. Infants were fed and wrapped and allowed to sleep naturally in the scanner. Pulse oximetry, temperature and heart rate were monitored throughout and ear protection was provided for each infant (President Putty, Coltene Whaledent, Mahwah, NJ; MiniMuffs, Natus Medical Inc., San Carlos, CA). T2-weighted images were acquired in two stacks of slices acquired in sagittal and axial planes using the following parameters: TR=12s, TE=156ms, SENSE factor 2.11 (axial) and 2.58 (sagittal) (Hughes et al., 2017). Overlapping slices (resolution $0.8 \times 0.8 \times 1.6 \text{ mm}^3$) were acquired to give a final upsampled image resolution of $0.5 \times 0.5 \times 0.5 \text{ mm}^3$ after reconstruction and motion correction (Kuklisova-Murgasova et al., 2012; Cordero-Grande et al., 2016, 2017). T1-weighted images were acquired using an inversion recovery sequence at the same resolutions with TI=1740ms, TR=4.8s, TE=8.7ms, SENSE factor 2.26 (axial) and 2.66 (sagittal). All images were reviewed by a paediatric neuroradiologist.

2.2 Adaptive kernel regression

Age-dependant atlases were constructed for 9 weeks (36 to 44 weeks PMA) using adaptive kernel regression (Serag et al., 2012). Kernel size is determined in an adaptive way and defines temporal smoothness, where for weeks with higher density of subjects, a smaller sigma is chosen, and for weeks with fewer subjects a larger sigma is chosen. The target number of subjects included in time-interval groups for averaging was derived by first defining a target kernel $\sigma = 1$ week, followed by measuring the median number of subjects included per age at this given σ and then adjusting the σ at each age in order to reach this target number of subjects. The age distribution of our dataset is shown in Fig 1. The resulting number of subjects in each time-interval group (from week 36 to week 44) were: 195, 195, 195, 198, 196, 197, 195, 195 and 195; with the resulting σ at each age: 1.64, 1.31, 1, 0.77, 0.64, 0.73, 0.9, 1.18 and 1.5 weeks. The numbers per template differ slightly as a resulting of avoiding splitting groups of subjects that were equidistant from the time interval center.

2.3 Pre-processing

All images were processed using dHCP Structural Pipelines described in (Makropoulos et al., 2018). This pipeline generates white matter, midthickness, pial, inflated, very inflated and spherical surfaces, which all have vertex correspondence, as well as summary feature maps describing sulcal depth, mean curvature, cortical thickness, cortical T1w/T2w myelin maps and cortical labels (Fig 2). For more complete details refer to (Makropoulos et al., 2018); however, in brief, sulcal depth maps represent mean convexity or concavity of a surface

(Fischl et al., 1999a); mean curvature represents measure of cortical folding estimated from the average of principle curvatures (white surface); cortical thickness is estimated based on the Euclidean distance between corresponding vertices of the white and pial surfaces; T1w/T2w myelin maps represent relative myelin content in the cortical ribbon obtained from the ratio of T1 and T2-weighted images (relevant details regarding T1w/T2w myelin maps computation are included in the Supplementary Material); and cortical regional labels are propagated from the regions obtained in the volumetric segmentation.

Prior to template generation all surfaces were pre-aligned, through estimation of a rigid transformation between each subject's T2w image and the infant volumetric template. This ensures all neonatal surfaces have the same orientation and centering. Further, we estimate, and apply to each individual surface, a rotation between previously developed template (Bozek et al., 2016), which was constructed in MNI space, and adult Conte69 atlas (Van Essen et al., 2012; Glasser and Van Essen, 2011), which is significantly rotated with respect to the MNI space, in order to initialise alignment. This is a similar approach to the one proposed in Van Essen et al. (2012), where a rotation is estimated between "fsaverage" space and Conte69 space and was used to initialise alignment.

2.4 Template Generation

We generate the neonatal surface template in two stages: creation of an initial template through affine, spherical registration to an adult atlas, followed by iterative refinement performed using MSM (Robinson et al., 2018).

In the first stage, each individual neonatal surface is initialised through affine, spherical alignment to the Conte69 atlas (Van Essen et al., 2012; Glasser and Van Essen, 2011). Here, matching is performed between sulcal depth maps as these reflect coarse scale folding patterns that are common between neonates and adults (see Fig 3). Optimal (affine) rotation parameters are estimated through gradient descent.

Following this, subject's mean sulcal depth features are resampled onto the template sphere, using barycentric interpolation. Initial sulcal depth template averages are then obtained by averaging within weeks using kernel weighting (section 2.4.1).

Affine initialisation, designed to generate an unbiased reference space, does not give a sharp feature result. The sulcal depth template captures coarse scale folding patterns across subjects, but it is unable to provide a representative average of all patterns of gyrification due to the high degree of cortical folding and variation in cortical folding patterns that has been observed in nature.

For this reason we refine the template via direct non-rigid MSM spherical alignment (Robinson et al., 2018) of all subjects to the average, over several iterations. Registration is driven using mean curvature features (Fig 4) as these reflect more fine scale patterns of folding. At each refinement iteration, average features from the previous iteration are used as reference features for registering individual spherical meshes to the template spherical mesh. Iterations stop when refinement of the feature maps converges. Fig 4 shows curvature at several iteration steps with vertex-wise difference of curvature maps in respect to the

previous iteration step. The change plateaus when the mean of absolute vertex-wise difference between subsequent iterations is 0.003.

In order to average surfaces and obtain anatomical and cortical feature templates, several steps are needed in order to map correspondences learnt during spherical alignment to cortical features and anatomies, and then perform averaging.

First, neonatal cortical anatomies are brought into approximate alignment by estimating an affine volumetric warp between each neonatal and the adult anatomical reference. This is achieved by resampling each neonatal cortical anatomy onto the adult reference mesh, taking advantage of the known vertex correspondence between each subject's sphere (which is in alignment with the reference sphere) and their anatomy (see (Robinson et al., 2018) for more details). This results in a resampled neonatal anatomical surface, with the shape of the adult cortical reference but the mesh topology (number of vertices) of the neonatal surface. Doing this generates point-wise correspondences (with original anatomies) through which affine transformation matrices are estimated, and applied, to bring all neonatal cortices into approximate alignment, prior to averaging. As a side effect, these surfaces are then scaled to the size of the reference Conte69 mesh.

Then, nonlinear correspondences between anatomical surfaces are assigned by resampling the reference mesh topology onto the estimated rescaled, reoriented anatomical surfaces, using correspondences learnt from the MSM spherical warp. This results in meshes with the same shape as the original neonatal cortical anatomies, but now with constant numbers of vertices and accurate vertex correspondence across individuals. These transformed surfaces can then be directly averaged to get each anatomical template.

Finally, individual feature maps are also resampled to the template, using correspondences learnt through the curvature defined mapping. These are averaged to generate population average templates of sulcal depth, curvature, thickness, and T1w/T2w myelin maps.

2.4.1 Template Average: adaptive kernel weighting—Final estimates of template surfaces and feature maps are obtained through adaptive kernel weighted averaging across all subjects' registered and resampled data. It follows the adaptive kernel weighting approach proposed for volumetric atlas construction in Serag et al. (2012), designed to address uneven dataset distribution.

Let S_i with $i = 1, \dots, m$, represent the source and C_T represent the reference (template) spherical mesh coordinates, A_i represent the source and A_T represent reference anatomical (white, pial, midthickness) surface mesh spaces, and D_i and D_T^{n-1} represent feature maps (sulcal depth, curvature, T1w/T2w myelin, thickness) for the source and the template obtained in iteration $n - 1$, respectively. The n th registration, for subject i , yields transformed spherical mesh S'_i , transformed anatomical (white, pial, midthickness) surface meshes A'_i (see section 2.4), and transformed data D'_i , obtained by resampling the aligned data onto the template, prior to averaging.

For each week the templates, that consist of a spherical and anatomical surface mesh and corresponding data, are obtained by weighted averaging:

$$\bar{S} = \frac{\sum_{i=1}^m w_i S'_i}{\sum_{i=1}^m w_i} \quad \bar{A} = \frac{\sum_{i=1}^m w_i A'_i}{\sum_{i=1}^m w_i} \quad \bar{D} = \frac{\sum_{i=1}^m w_i D'_i}{\sum_{i=1}^m w_i} \quad (1)$$

where w_i is a temporal weight defined by the difference between age t_i of the source subject and the age of the template, t , given by a Gaussian kernel

$$w_i = \frac{1}{\sigma\sqrt{2\pi}} \exp\left(\frac{-(t_i - t)^2}{2\sigma^2}\right) \quad (2)$$

where σ defines temporal smoothness and is determined in an adaptive way (Serag et al., 2012), described in section 2.2.

Cortical labels are resampled onto the final template mesh and labels of the different subjects are then combined with weighted averaging to generate a probabilistic map for each label. A maximum-probability atlas is obtained by assigning the label with the maximum probability at each vertex of the template mesh. It should be noted that maximum probability at each vertex does not explicitly preserve the topology of the parcels, and thus the method itself does not guarantee against holes in the segmentation. Nevertheless, in this instance (see exemplar probabilistic maps for cortical regions for week 40 in the Supplementary Material) we find the resulting topology is correct i.e. there are no holes within the parcels. This may be due to the relatively coarse nature of the parcels, which broadly follow patterns of coarse scale folding that are known to be consistent across individuals. For more fine grained and detailed parcellations, however, label fusion methods such as the ones proposed by Heckemann et al. (2006) and Aljabar et al. (2009) might prove more accurate.

2.4.2 De-drifting and Rescaling—Finally, all estimated templates are de-drifted and rescaled (to remove the impact of the initial mean scaling to the size of the adult atlas). Here, group average drift is a phenomenon that occurs when registration templates are being generated with non-rigid registration algorithms or when different registration algorithms or templates are used to drive alignment to a common standard space (Learned-Miller, 2006; Balci et al., 2007; Abdollahi et al., 2014). Drift is removed by computing the group average of subject meshes and concatenating its inverse onto each individual subject's registration. Following that, we repeated the weighted averaging in order to obtain a de-drifted template. Finally, we removed scaling, introduced through affine initialisation to the adult Conte69 atlas, by performing Log-Euclidian averaging of the affine transformations (Kuklisova-Murgasova et al., 2011), and then applying their inverse to the neonatal template to scale the template back to the size of an infant.

3 Results

3.1 Final atlases

The final anatomical cortical surface atlases for the white matter and pial surfaces for weeks 36 through 44 are shown in Figs 5 and 6. Cortical labels propagated to the final template and projected on the cortical pial surface for left hemisphere are shown in Fig 7 and for right hemisphere in Fig S5 in the Supplementary Material.

Final feature templates for left hemisphere for weeks 36 through 44 for mean curvature are shown in Fig 8, for sulcal depth maps in Fig 9, for cortical thickness in Fig 10 and for T1w/T2w myelin maps in Fig 11. The respective figures for the right hemisphere are included in the Supplementary Material (Figs S1-S4).

3.2 Atlas analysis

Templates are analysed in terms of spread, across subjects, of the average of feature values within each cortical region, for 32 cortical regions segmented with Draw-EM (Makropoulos et al., 2014) (based on the 20 atlases of (Gousias et al., 2012)). Specifically, mean value of a feature within each cortical region of each subject was input to kernel-weighted averaging to get the spread across subjects, shown in plots in Figs 12, 13, 14, 15 for sulcal depth, curvature, thickness, and T1w/T2w myelin maps, respectively, with error bars representing weighted standard deviation. The same analysis, but across the whole brain, not per region, is plotted in Fig 16 and presents mean template feature values computed as weighted average across subjects, with error bars representing weighted standard deviation. The figure also shows mean feature values across the whole brain for individual subjects. Supplementary Material provides complementary tables with listed average regional feature values and their change across weeks.

3.2.1 Cortical folding increases—Sulcal depth (Fig 12 and Fig S1) and curvature maps (Fig 13 and Fig S2) show a small increasing trend over the observed weeks in different regions, as the majority of folds are present at term age and are getting deeper. Across the whole brain the average of absolute sulcal depth changes for 13%, from 3.13 at 36 weeks to 3.52 at 44 weeks. Average of absolute curvature changes less than 1%, only from 1.65 (36 weeks) to 1.66 (44 weeks).

3.2.2 Cortical thickness growth—Thickness is also following an increasing trend across weeks, which can be observed in Fig 10 and Fig S3. This is expected since cortical thickness has a rapid increase in the neonatal period and during early childhood (Lyll et al., 2015; Dubois and Dehaene-Lambertz, 2015). Overall, our results show that the average thickness across the whole brain has a 6% increase, from 1.04 mm at 36 weeks to 1.10 mm at 44 weeks. Cumulative sum of percent change across the whole brain between weeks is plotted in Fig. 17 and follows growth trends reported in previous studies (Lyll et al., 2015; Makropoulos et al., 2016).

Values and percentage change of the average cortical thickness across subjects, per region and per whole brain are provided in tables in the Supplementary Material. There are regional variations in cortical thickness, with thinner regions being occipital and parietal lobes, while

thicker cortices include temporal regions. There is a regionally heterogeneous growth in the cortical thickness from 36 to 44 weeks. Regions experiencing the greatest increase of cortical thickness in the observed period include occipitotemporal gyri and insula. Regions experiencing the least increase include posterior cingulate gyrus, superior temporal gyrus and anterior temporal lobe.

3.2.3 T1w/T2w myelin increase—An increasing developmental trend for both hemispheres can also be observed in T1w/T2w myelin maps (Fig 11 for left and Fig S4 in the Supplementary Material for right hemisphere). Its average value across the whole brain increases 21%, from 1.04 (36 weeks) to 1.26 (44 weeks). Cumulative sum of percent change across the whole brain between weeks is plotted in Fig. 17 and tables with regional values and percentage change in T1w/T2w myelin across weeks are included in the Supplementary Material.

However, since the analysed regions include both areas of poor myelination and of high myelination (e.g. precentral gyrus which is analysed as a part of frontal lobe), the quantitative values may not depict the true developmental trends and a detailed regional segmentation should be analysed in the future. Highly myelinated regions seem to be occipital lobe, frontal lobe and superior temporal gyrus, while the least myelinated regions are gyri parahippocampalis et ambiens anterior and posterior, posterior cingulate gyrus and lateral occipitotemporal gyrus fusiformis anterior and posterior.

There is a regionally heterogeneous increase in T1w/T2w myelination from 36 to 44 weeks. The greatest increase in T1w/T2w myelination is in gyri parahippocampalis et ambiens posterior, posterior cingulate gyrus and lateral occipitotemporal gyrus fusiformis posterior. Regions experiencing the least increase include superior temporal gyrus middle, anterior temporal lobe and gyri parahippocampalis et ambiens anterior.

3.2.4 Cortical surface expansion—Surface area measure was used to assess expansion of the brain and of the different regional structures in the period across 36 to 44 weeks. It was computed by adding up the area of all triangular faces within each region of the pial surface. Plots of regional surface area measure are presented in Fig. 18, representing weighted average across subjects with error bars showing the weighted standard deviation. Results across the whole brain are plotted in Fig 19 and present mean surface area values computed as weighted average across subjects, with error bars representing weighted standard deviation. The figure also shows mean surface area across the whole brain for individual subjects.

Overall, our results show that the average cortical surface area across the whole brain has a 27% increase for left hemisphere, from 83,777 mm² at 36 weeks to 106,631 mm² at 44 weeks, and 28% increase for right hemisphere, from 81,792 mm² at 36 weeks to 104,689 mm² at 44 weeks. Cumulative sum of percent change across the whole brain between weeks is plotted in Fig. 17 and tables with regional values and percentage change in surface area across weeks are included in the Supplementary Material. The expansion trends follow growth reported in previous studies (Lyall et al., 2015; Makropoulos et al., 2016; Garcia et al., 2018). There are regional variations in the surface area expansion. Regions with high

expansion in the observed period are anterior temporal lobe medial, medial and inferior temporal gyri posterior and anterior, lateral occipitotemporal gyrus fusiformis anterior and frontal lobe. Low-expanding regions include gyri parahipp. et ambiens posterior and anterior, insula and cingulate gyrus posterior and anterior, with cingulate gyrus anterior showing a 15% decrease in left hemisphere.

3.2.5 Gyrfication index—The increasing trajectory of growth is shown in Fig 20 by calculating gyrfication indices (GI) for brains of individual subjects and for the final atlas. GI is defined as $GI = Area_{pial}/Area_{hull}$, where $Area_{pial}$ is the surface area of the pial surface and $Area_{hull}$ is the surface area of the convex hull surface, which is obtained by morphologically closing the pial surface. In individual cases, gyrfication index ranges from 1.73 at 36 weeks to 2.86 at 44 weeks for left hemisphere and from 1.74 at 36 weeks to 2.83 at 44 weeks for right hemisphere. Weighted average across individual subjects ranges from 2.09 at 36 weeks to 2.57 for 44 weeks for left hemisphere and from 2.08 at 36 weeks to 2.58 for 44 weeks for right hemisphere.

It should be noted that due to the smoothing of gyri during surface averaging, which is due to intersubject variability, the group average surfaces have less defined folding, making measures such as gyrfication index less meaningful on average surfaces (here, 1.45 at 36 weeks to 1.60 at 44 weeks for left hemisphere and 1.41 at 36 weeks to 1.60 at 44 weeks for right hemisphere).

3.3 Inter-hemispheric asymmetries

Developmental growth trends are similar in both hemispheres, however, some asymmetries between left and right hemispheres can be observed in some regions. Sulcal depth has higher values of anterior temporal lobe medial and lateral in left hemisphere compared to the right, while lower values in superior temporal gyrus middle, lateral occipitotemporal gyrus fusiformis anterior, insula and gyri parahipp. et ambiens posterior. There is not much inter-hemispheric asymmetry in mean curvature, except in insula which has greater mean curvature in right hemisphere. This was also observed in the studies of the adult healthy brains (Kang et al., 2012).

There are some regional asymmetries between left and right hemisphere in the mean thickness. Cortical thickness is higher in left hemisphere in anterior temporal lobe medial and lateral occipitotemporal gyrus fusiformis, while greater in right hemisphere in gyri parahippocampalis et ambiens anterior. Increase of thickness from 36 to 44 weeks across the whole brain for left and right hemispheres is plotted in Fig. 17 and shows cumulative sum of percent change between weeks.

Asymmetry between hemispheres is prominent in T1w/T2w myelin, with higher myelination in right hemisphere in anterior temporal lobe medial and lateral, and gyri parahippocampalis et ambiens anterior. There is no asymmetry in the increase of myelination of hemispheres (21% increase from 36 to 44 weeks). This can also be observed in Fig. 17 where left and right hemisphere growth curves overlap.

Left hemisphere has a bigger cortical surface area (83,777 mm² at 36 weeks and 106,631 mm² at 44 weeks) compared to the right hemisphere (81,792 mm² at 36 weeks and 104,689 mm² at 44 weeks). However, cortical expansion is marginally greater in right hemisphere, where from 36 to 44 weeks surface area increases 28% in the right hemisphere compared to the 27% increase of the left hemisphere.

3.4 Distortion maps

To evaluate the biological plausibility of the deformations estimated during alignment, areal distortion map is computed for each subject and the absolute values of areal distortion are averaged across subjects within each week. Areal distortion is defined as $\log_2(Area_1/Area_2)$, where $Area_1$ is the area of the registered spherical surface tile and $Area_2$ is the area of the original spherical surface tile. Also, we computed average across subjects of the anisotropic deformation map. The anisotropic deformation map or anisotropic strain is calculated by an affine transform between matching triangles, and then averaged across the triangles of a vertex. It is defined as $AS = \log_2(SR_{max}/SR_{min})$, where SR_{max} is major stretch ratio and SR_{min} minor stretch ratio between the registered and original spherical surface tile pair, if affine registration is applied to the pair. It represents how elongated a unit circle would become, i.e. if the unit circle is transformed to an ellipse with major axis 2 and minor axis 1/2, then the anisotropic strain is 4. Areal distortion and anisotropic strain are computed using Connectome Workbench³ command `-surface-distortion` with `-local-affine-method` option (developers version May 2017).

The averaged absolute areal distortion map and the averaged anisotropic deformation map spanning 36 to 44 weeks are shown in Figs 21 and 22. Mean of the average across subjects of the absolute areal distortion map is 0.18 for left and 0.17 for right hemisphere, and mean of the anisotropic distortion map is 0.45 for left and 0.47 for right hemisphere. Peak distortions (maximum and minimum values) of the entire dataset are listed in Table 1. Table 2 lists mean areal and anisotropic distortions across all subjects and all weeks and its maximum values to facilitate comparison with values reported in prior study by Robinson et al. (2018), where distortions measured folding based alignment of the adult HCP task fMRI data using spherical MSM with higher-order strain regularisation ($sMSM_{STR}$).

Increased areal distortion is observed around the Sylvian fissure and in the inferior parietal lobe on the lateral side. On the medial wall it is increased in the occipital lobe and in the ventromedial prefrontal areas. Mean areal distortion in this study is 0.17 (prior study 0.102) and its maximum is 0.68 (prior study 0.525).

The anisotropic deformation map exhibits higher values compared to areal distortion, although still smooth across the surface. It has similar pattern to the one reported in Robinson et al. (2018). However, our distortion values are higher, because the prior study optimised the regularization of the folding alignment so as to maximize alignment of cortical areas as measured using task fMRI rather than maximizing alignment of cortical folds (and thereby reducing the alignment of cortical areas somewhat). Mean anisotropic distortion in this study is 0.46 (prior study 0.235) with maximum value of 2.20 (prior study 1.151). Due

³<http://www.humanconnectome.org/software/connectome-workbench>

to higher values, scale of mean anisotropic distortion in Fig 22 is 0.0-1.0, compared to prior study where the scale was 0.0-0.5.

4 Discussion

This paper presents the first spatio-temporal neonatal cortical surface atlas for 36 to 44 weeks PMA, collected using data from the developing Human Connectome Project. Templates reflect both mean geometry (shape), cortical folding, thickness, and T1w/T2w myelination, and estimate per week averages of cortical regions (defined using the ALBERT's atlas (Gousias et al., 2012)).

The atlas retains features that are representative of the subject population and provides a sharp template for the cortical surface analysis and for visualisation purposes. Additionally, the atlas shows developmental trends of cortical features, including some increase in the complexity of cortical folding, and increase in thickness and in T1w/T2w myelination. Finally, analysis of cortical features in corresponding regions of left and right hemisphere investigates symmetry between the two hemispheres.

Developmental trends across weeks can be recognised in the cortical thickness feature which increases with age (Fig 17). Although the developmental trends of cortical thickness at the neonatal period are still not thoroughly investigated, in the first postnatal year there is robust and regionally heterogeneous growth of cortical thickness averaging 31% (Lyall et al., 2015). Our cortical thickness data indicates small increases in cortical thickness over the immediate post-natal weeks. The large, regionally heterogeneous, increase that occurs in the first post-natal years is not apparent yet in our age range. In addition, our cortical thickness values are significantly lower than those seen in other samples, with our ranges lying just above 1 mm on average, whereas other recent studies show values centred around 2 mm (Li et al., 2016). However, differences between reported values can be due to different image acquisition, image segmentation and surface reconstruction methods, as discussed in Makropoulos et al. (2018). Moeskops et al. (2013) present thickness values estimated based on manually segmented cortices and the estimated thickness in their study varies between 0.95 and 1.2 mm which is very similar to the obtained measurements here. Further, the histological findings by Moore and Guan (2001) indicate thickness of about 1.2 mm at 37-42 weeks in Heschl's gyrus, increasing rapidly thereafter.

Studies focusing on the first postnatal years such as Lyall et al. (2015) demonstrate much more dramatic changes in cortical thickness, mirroring the large overall brain growth, synaptic and dendritic proliferation (Huttenlocher and Dabholkar, 1997) and reflecting more widespread myelination of the underlying white matter, all co-occurring at a fast rate in the first postnatal year in particular. Our results are relatively subtle, regional patterns of cortical thickness growth obtained through the analysis of our dataset (36 to 44 weeks PMA) were very similar to the ones observed in the first 2 years of life in the study performed by Lyall et al. (2015). We found that regions with the greatest increase of cortical thickness include occipitotemporal gyri and insula. Similarly, Lyall et al. (2015) determined that in the first two years of life one of the regions with the greatest thickness growth is insula.

Further, they found that regions with the least amount of thickness growth were postcentral gyrus, superior parietal gyrus, multiple areas in the occipital lobe and the middle temporal pole, while our analysis observed the least increase in posterior cingulate gyrus, superior temporal gyrus and anterior temporal lobe. This may suggest that there are developmental trends in the period around term age that are similar to the first two years of development. Longitudinal follow-up and a wider age range would help to provide greater insight in this very dynamic period of brain development.

Another feature that was captured in the template and that followed brain development that can be observed in the individual subjects is myelin. Myelin is seen microscopically from 35 weeks of post-menstrual age in the pre- and postcentral gyri (Rutherford, 2002). Although in the literature T1w/T2w myelin maps were mostly used in the adult brain analysis, the T1w/T2w ratio can be used to assess myelination in the neonatal population (Soun et al., 2016). T1w/T2w myelin maps relate to the areal boundaries (Glasser and Van Essen, 2011) of cortical areas and mapping cortical myelin content in the neonatal brain could improve the ability to diagnose myelin abnormalities in the developing brain, since they are sensitive to myelin density in neonates, as they are in adults (Soun et al., 2016). The use of HCP-standard cortical T1w/T2w myelin maps is chosen to allow comparison with adult HCP data, and also on account the choice of scans available through the dHCP protocol (Makropoulos et al., 2018). Within this limitation, it is important to note that the neonatal myelin maps were generated from a IR-TSE T1 sequence, rather than the MPRAGE as used in Glasser and Van Essen (2011). T1w/T2w myelin maps computed for the final templates showed a general trend of increase of myelination across weeks, with the expected heavier myelination in primary cortical areas: pre- and post-central gyri (motor-somatosensory), calcarine sulcus (visual) and Heschl gyrus (auditory) (Glasser and Van Essen, 2011). Across the whole brain there was a 21% increase in T1w/T2w myelin maps from 36 to 44 weeks. There is a limitation in our regional analysis of myelination trends due to the size of our regions. Since some of the regions are big, the effect of the high T1w/T2w myelin in regions such as precentral gyri gets averaged in with regions of low myelin in frontal cortex, and similarly happens with postcentral gyri being averaged within parietal areas.

Developmental growth was also assessed using the measure of cortical surface area. Its expansion showed agreement with previous studies (Lyll et al., 2015; Makropoulos et al., 2016). Week 37 is considered early term age (American College of Obstetricians and Gynecologists, 2013) and the fastest brain growth occurs before 36 weeks, after which the growth rate decreases (Armstrong et al., 1995). However, patterns of cortical folding obtained in the template agree with the fact that, by early term age, sulci are formed and over the following few term weeks they become deeper (Rutherford, 2002). Admittedly, not having atlases for fetal population at the moment is a potential limitation of this study and a constraint on the analysis of the development trends. However, the template method will be extended to fetal groups once we acquire the data.

The gyrification index showed the increase of the fine scale folding across the weeks, where our templates followed the general trend towards increased gyrification index which reflects the pattern observed in the individual subjects. The values of the gyrification index of our final atlas are smaller on average than the ones measured in post-mortem brains in

Armstrong et al. (1995), where values ranged from 2.0 (at around 36 weeks of age) to 2.3-2.8 (at around 44 weeks of age). Also, as presented in the results section 3.2.5 they are smaller than the values estimated from the individual cases from our dataset. The reason for smaller values estimated for the final template is likely due to smoothing of the smaller and finer folds during the averaging process. This is a common, unavoidable, side-effect of brain atlasing procedures, resulting from considerable inter-subject variability in cortical shape.

We have analysed inter-hemispheric asymmetries present in the template features (cortical folding, thickness, T1w/T2w myelin) as well as in the cortical surface area. Our results revealed inter-hemispheric asymmetries present at this early stage of the development, which are consistent with previous studies. As summarized by (Toga and Thompson, 2003) there are regional differences between the two hemispheres, although they are similar in weight and volume. Some of the studies of inter-hemispheric asymmetries, such as the one by (Dubois et al., 2008) and Van Essen (2005) focused on the asymmetry of sulci. As reported for preterm born neonates (Dubois et al., 2008), the right hemisphere presents gyral complexity earlier than the left, with a larger superior temporal sulci for most preterm newborns. This was also observed in our results, where sulcal depth had larger values for right hemisphere in the superior temporal region. The T1w/T2w myelin asymmetries observed in our data should be taken with caution, due to the size of our regions. Further evidence and analysis are needed to determine whether the observed inter-hemispheric asymmetry is indeed genuine.

The biological plausibility of deformations estimated during the alignment was assessed using areal distortion and anisotropic strain. Areal distortion is higher in the left hemisphere compared to the right, which may have biased our analysis of inter-hemispheric asymmetries. In the adult population used in Robinson et al. (2018) there are also present some inter-hemispheric asymmetries of areal distortion, although the analysis was performed only on 28 adult subjects and thus those asymmetries should be taken with caution. The deformations in our data across the cortical surface are higher, but comparable in pattern, with the ones reported for adults in Robinson et al. (2018). However, folding alignment in Robinson et al. (2018) was optimized in order to maximise alignment of task fMRI. Thus, although our distortions are higher, they are in a biologically plausible range. Biologically plausible distortion is a source of differing opinions for folding-based registration and is an open question in the research community. However, it is considered that biological plausibility means that the distortions are lower than 4-fold expansion or compression (Van Essen, 2005).

In this paper initial template construction is based on affine alignment of all individuals to Conte69 (Van Essen et al., 2012). Initialisation towards adult atlas allows for future comparisons across different populations, namely neonatal and adult, as well as comparisons of neonatal data against data and results obtained in HCP studies.

It is important to point out that using adult atlas as a volumetric reference introduces bias of the neonatal atlas towards the adult space, and it alters the size of the brain. We have removed this bias and rescaled the templates to the neonatal brain size by following the approach presented in Kuklisova-Murgasova et al. (2011), where affine transformations are

averaged using Log-Euclidian averaging and their inverse is applied to the neonatal template.

In order to account for the drifting of the spherical atlas features that occurred during the refinement through iterative registrations, we removed the drift by computing the group average and concatenating its inverse onto each individual subject's registration, after which we computed the new de-drifted average.

Coarse scale folding features, namely sulcal depth maps, are used to drive the affine registrations, since finer scale cortical folding features, such as curvature, have a high degree of inter-subject variability, and these were used for atlas refinement (Hill et al., 2010). Iterative atlas refinement follows a commonly utilised approach of aligning subjects to the template from the previous step and averaging the results to obtain a refined template until it converges (Fischl et al., 1999b; Black et al., 2001; Lyttelton et al., 2007).

The temporal resolution depends on the amount of available data for each time interval, and the difference between the age of subjects and the age of each template. These limitations could have been overcome by using adaptive kernel regression (Serag et al., 2012), diffeomorphic regression (Singh and Niethammer, 2014) or statistical growth regression (Durrleman et al., 2013). We used adaptive kernel weighted averaging (Serag et al., 2012), where the kernel serves to interpolate between the subjects and to average out the inter-subject variation. Using kernel regression we achieved an overlap, and hence continuity, of subjects, where subjects whose age was further away from the template age were given a smaller weight in the averaging process. Since our dataset had an uneven distribution of cases across weeks, in order to eliminate possible dataset size bias, we used adaptive kernel weight for averaging. For weeks with higher density of subjects, a smaller temporal smoothness is chosen, and for weeks with fewer subjects a larger temporal smoothness is chosen. The used target kernel width and obtained number of subjects per week produced temporally smooth atlases with noticeable shape differences. It is likely that significantly increasing the number of subjects in each time interval would impact the atlas shape and feature maps by making them smoother, thereby failing to model the temporal shape differences.

An alternative approach for averaging used by Wright et al. (2015), which is also based on Serag et al. (2012), uses fixed temporal kernel width across weeks because of fairly evenly distributed subjects in their dataset. Further, besides the temporal weighting, their weighting function included spatial weighting. Spatial weighting was used to find the average surface position and achieve uniform spatial smoothness, because the vertices of each surface were not evenly sampled in the domain they used to build the templates.

Using spherical registration, such as MSM, our neonatal atlas has the potential to be brought into alignment with other neonatal surface atlases that are based on a spherical projection containing cortical features, such as the aforementioned Hill et al. (2010), Li et al. (2015) and Wright et al. (2015). In this way, the atlases could be used in a complementary fashion, and extend the time-interval in which brain development is analysed.

There are limitations with this approach inasmuch as, even at these early developmental stages, a single population atlas might not be able to capture and show all individual variations in a population due to the anatomical variability across subjects (Bijsterbosch et al., 2018). Hence the group average surfaces are smoother, with shallower folds than those of individuals. Currently there are no clear alternatives for creating templates that reflect inter-subject variability. Although, there is a potential for methods such as those proposed by Wang et al. (2015), which make use of use intermediate templates or (Jordan et al., 2016), which combine global spatially constrained alignment with local hyper-alignment techniques. Another possible fix might be the use of groupwise methods such as (Robinson et al., 2016), where this is performed through a discrete optimisation framework that seeks to simultaneously improve pairwise correspondences between surface feature sets, while minimising a global cost relating to the rank of the features.

The cortical surface atlas can be used to compare functional and diffusion MRI outputs. However, folding-based alignment is not the optimal way to align functional data, though it can be tuned for that purpose. We have previously shown that using more stringent distortion regularisation of folding-based alignment produced better functional alignment at the expense of more residual folding variability (Robinson et al., 2014). Additionally, driving surface alignment with functionally relevant features produces even more folding variability, while improving functional alignment (Glasser et al., 2016a). The reason for these effects is the often poor correlation between folding patterns and cortical areas (Glasser et al., 2016b). Thus, this folding aligned template may have more folding detail than would be present in a functionally aligned template of these same data. In general, it is best to align all data in a given study using the same registration approach, and not, for example, to display functionally aligned data on a folding aligned template. Thus, future work will focus on optimising the framework for functional alignment, which would be a natural next step once we have the data.

In conclusion, our proposed atlas (available to download from <http://brain-development.org/brain-atlases/cortical-surface-atlas>) represents the first spatio-temporal atlas based on cortical surfaces of the developing brain around term age. It provides means of comparing a wide variety of features on the cortical surface and a vital resource for comparing and contrasting multimodal imaging data on the cortical surface, as well as for a population based study to compare brain structure and folding across populations and over time. Future work will extend the template to preterm and fetal cohorts.

Supplementary Material

Refer to Web version on PubMed Central for supplementary material.

Acknowledgements

The research leading to these results has received funding from the European Research Council under the European Union's Seventh Framework Programme (FP/2007-2013) / ERC Grant Agreement no. 319456. This work was supported by the the National Institute for Health Research (NIHR) Oxford Biomedical Research Centre (BRC). This work was supported by the NIHR Comprehensive Biomedical Research Centre award to Guy's & St Thomas' NHS Foundation Trust in partnership with King's College London and Kings College Hospital NHS Foundation Trust. Dr Robinson is supported by the Wellcome EPSRC Centre for Medical Engineering at Kings College London

(WT 203148/Z/16/Z). We are thankful to our colleagues from the Developing Human Connectome Project recruitment, radiography and research nurse team.

References

- Abdollahi R, Kolster H, Glasser M, Robinson E, Coalson T, Dierker D, Jenkinson M, Van Essen D, Orban G. Correspondences between retinotopic areas and myelin maps in human visual cortex. *NeuroImage*. 2014 Oct.99:509–524. [PubMed: 24971513]
- Aljabar P, Heckemann RA, Hammers A, Hajnal JV, Rueckert D. Multi-atlas based segmentation of brain images: Atlas selection and its effect on accuracy. *NeuroImage*. 2009 Jul.46:726–738. [PubMed: 19245840]
- American College of Obstetricians and Gynecologists. Definition of term pregnancy. Committee Opinion No. 579. *Obstetrics and Gynecology*. 2013 Nov.122:1139–40. [PubMed: 24150030]
- Armstrong E, Schleicher A, Omran H, Curtis M, Zilles K. The ontogeny of human gyrification. *Cerebral Cortex*. 1995 Jan-Feb;5:56–63. [PubMed: 7719130]
- Balci SK, Golland P, Wells W. Non-rigid groupwise registration using b-spline deformation model. Open source and open data for MICCAI. 2007
- Bijsterbosch JD, Woolrich MW, Glasser MF, Robinson EC, Beckmann CF, Van Essen DC, Harrison SJ, Smith SM. The relationship between spatial configuration and functional connectivity of brain regions. *eLife*. 2018 Feb.7:e32992. [PubMed: 29451491]
- Black KJ, Snyder AZ, Koller JM, Gado MH, Perlmutter JS. Template images for nonhuman primate neuroimaging. 1. Baboon. *International Journal of Computer Vision*. 2001 May.14:736–743.
- Bozek, J; Fitzgibbon, S; Wright, R; Rueckert, D; Jenkinson, M; Robinson, E. Construction of a neonatal cortical surface atlas using multimodal surface matching. 2016 IEEE International Symposium on Biomedical Imaging: From Nano to Macro; 2016. 775–778.
- Cordero-Grande L, Hughes E, Hutter J, Price A, Hajnal JV. Three-dimensional motion corrected sensitivity encoding reconstruction for multi-shot multi-slice mri: Application to neonatal brain imaging. *Magnetic Resonance in Medicine*. 2017
- Cordero-Grande L, Teixeira R, Hughes E, Hutter J, Price A, Hajnal J. Sensitivity encoding for aligned multishot magnetic resonance reconstruction. *International Journal of Computer Vision*. 2016 Sep. 2:266–280.
- Dubois J, Benders MAC, Lazeyras F, Leuchter RH-V, Sizonenko SV, Borradori-Tolsa C, Mangin JF, Hppi PS. Mapping the early cortical folding process in the preterm newborn brain. *Cerebral Cortex*. 2008 Jun.18:1444–1454. [PubMed: 17934189]
- Dubois, J, Dehaene-Lambertz, G. Fetal and Postnatal Development of the Cortex: MRI and Genetics. Vol. 2. Academic Press; Elsevier: 2015. 11–19.
- Durrleman S, Pennec X, Trouv A, Braga J, Gerig G, Ayache N. Toward a comprehensive framework for the spatiotemporal statistical analysis of longitudinal shape data. *International Journal of Computer Vision*. 2013 May.103:22–59. [PubMed: 23956495]
- Evans, AC; Collins, DL; Mills, SR; Brown, ED; Kelly, RL; Peters, TM. 3D statistical neuroanatomical models from 305 MRI volumes. *Proc IEEE-Nuclear Science Symposium and Medical Imaging Conference*; 1993. 1813–1817.
- Fischl B, Rajendran N, Busa E, Augustinack J, Hinds O, Yeo BT, Mohlberg H, Amunts K, Zilles K. Cortical folding patterns and predicting cytoarchitecture. *Cerebral Cortex*. 2008; 18(8):1973–1980. DOI: 10.1093/cercor/bhm225 [PubMed: 18079129]
- Fischl B, Sereno M, Dale A. Cortical surface-based analysis. II: Inflation, flattening, and a surface-based coordinate system. *NeuroImage*. 1999a Feb.9:195–207. [PubMed: 9931269]
- Fischl B, Sereno M, Tootell R, Dale A. High-resolution intersubject averaging and a coordinate system for the cortical surface. *Human Brain Mapping*. 1999b Nov.8:272–284. [PubMed: 10619420]
- Garcia KE, Robinson EC, Alexopoulos D, Dierker DL, Glasser MF, Coalson TS, Ortinau CM, Rueckert D, Taber LA, Van Essen DC, Rogers CE, et al. Dynamic patterns of cortical expansion during folding of the preterm human brain. *Proceedings of the National Academy of Sciences*. 2018

- Glasser MF, Sotiropoulos S, Wilson J, C TS, Fischl B, Andersson J, Xu J, Jbabdi S, Webster M, Polimeni J, Van Essen D, et al. The minimal preprocessing pipeline for the human connectome project. *NeuroImage*. 2013 Oct.80:105–124. [PubMed: 23668970]
- Glasser M, Van Essen D. Mapping human cortical areas in vivo based on myelin content as revealed by T1- and T2-weighted MRI. *The Journal of Neuroscience*. 2011 Aug.31:11597–616. [PubMed: 21832190]
- Glasser MF, Coalson TS, Robinson EC, Hacker CD, Harwell J, Yacoub E, Ugurbil K, Andersson J, Beckmann CF, Jenkinson M, Smith SM, et al. A multi-modal parcellation of human cerebral cortex. *Nature*. 2016a Aug.536:171–178. [PubMed: 27437579]
- Glasser MF, Smith SM, Marcus DS, Andersson JLR, Auerbach EJ, Behrens TEJ, Coalson TS, Harms MP, Jenkinson M, Moeller S, Robinson EC, et al. The human connectome project's neuroimaging approach. *Nature Neuroscience*. 2016b Sep.19:1175–1187. [PubMed: 27571196]
- Gousias I, Edwards A, Rutherford M, Counsell S, Hajnal J, Rueckert D, Hammers A. Magnetic resonance imaging of the newborn brain: Manual segmentation of labelled atlases in term-born and preterm infants. *NeuroImage*. 2012 Sep.62:1499–1509. [PubMed: 22713673]
- Guimond A, Meunier J, Thirion J-P. Average brain models: A convergence study. *Computer vision and image understanding*. 2000 Feb.77:192–210.
- Heckemann RA, Hajnal JV, Aljabar P, Rueckert D, Hammers A. Automatic anatomical brain mri segmentation combining label propagation and decision fusion. *NeuroImage*. 2006 Oct.33:115–126. [PubMed: 16860573]
- Hill J, Dierker D, Neil J, Inder T, Knutsen A, Harwell J, Coalson T, Essen DV. A surface-based analysis of hemispheric asymmetries and folding of cerebral cortex in term-born human infants. *The Journal of Neuroscience*. 2010 Feb.30:2268–76. [PubMed: 20147553]
- Hughes, E; Cordero-Grande, L; Murgasova, M; Hutter, J; Price, A; Gomes, ADS; Allsop, J; Steinweg, J; Tusor, N; Wurie, J; Bueno-Conde, J; , et al. The Developing Human Connectome: announcing the first release of open access neonatal brain imaging. 23rd Annual Meeting of the Organization for Human Brain Mapping; 2017.
- Hughes EJ, Winchman T, Padormo F, Teixeira R, Wurie J, Sharma M, Fox M, Hutter J, Cordero-Grande L, Price AN, Allsop J, et al. A dedicated neonatal brain imaging system. *Magnetic Resonance in Medicine*. 2016; doi: 10.1002/mrm.26462
- Huttenlocher P, Dabholkar A. Regional differences in synaptogenesis in human cerebral cortex. *The Journal of Comparative Neurology*. 1997 Oct.387
- Jordan MC, Joulin A, Beck DM, Fei-Fei L. Locally-optimized inter-subject alignment of functional cortical regions. *arXiv preprint arXiv:1606.02349*. 2016
- Kang X, Herron TJ, Cate AD, Yund EW, Woods DL. Hemispherically-unified surface maps of human cerebral cortex: Reliability and hemispheric asymmetries. *PLoS One*. 2012 Sep.7:e45582. [PubMed: 23029115]
- Kuklisova-Murgasova M, Aljabar P, Srinivasan L, Counsell S, Doria V, Serag A, Gousias I, Boardman J, Rutherford M, Edwards A, Hajnal J, et al. A dynamic 4D probabilistic atlas of the developing brain. *NeuroImage*. 2011 Feb.54:2750–63. [PubMed: 20969966]
- Kuklisova-Murgasova M, Quaghebeur G, Rutherford M, Hajnal J, Schnabel J. Reconstruction of fetal brain mri with intensity matching and complete outlier removal. *Medical Image Analysis*. 2012 Dec.16:1550–1564. [PubMed: 22939612]
- Learned-Miller EG. Data driven image models through continuous joint alignment. *IEEE Transactions on Pattern Analysis and Machine Intelligence*. 2006 Feb; 28(2):236–250. [PubMed: 16468620]
- Li G, Wang L, Shi F, Gilmore J, Lin W, Shen D. Construction of 4D high-definition cortical surface atlases of infants: Methods and applications. *Medical Image Analysis*. 2015 Oct.25:22–36. [PubMed: 25980388]
- Li G, Wang L, Shi F, Lyall A, Ahn M, Peng Z, Zhu H, Lin W, Gilmore J, Shen D. Cortical thickness and surface area in neonates at high risk for schizophrenia. *Brain Structure and Function*. 2016 Jan.22:447–461. [PubMed: 25362539]
- Lombaert, H, Sparring, J, Siddiqi, K. *Diffeomorphic Spectral Matching of Cortical Surfaces*. Springer Berlin Heidelberg; Berlin, Heidelberg: 2013. 376–389.

- Lyall AE, Shi F, Geng X, Woolson S, Li G, Wang L, Hamer RM, Shen D, Gilmore JH. Dynamic development of regional cortical thickness and surface area in early childhood. *Cerebral Cortex*. 2015; 25(8):2204–2212. DOI: 10.1093/cercor/bhu027 [PubMed: 24591525]
- Lytelton O, Boucher M, Robbins S, Evans A. An unbiased iterative group registration template for cortical surface analysis. *NeuroImage*. 2007 Feb.34:1535–1544. [PubMed: 17188895]
- Makropoulos A, Aljabar P, Wright R, Hning B, Merchant N, Arichi T, Tusor N, Hajnal J, E AD, Counsell S, Rueckert D. Regional growth and atlasing of the developing human brain. *NeuroImage*. 2016 Jan.125:456–478. [PubMed: 26499811]
- Makropoulos A, Gousias I, Ledig C, Aljabar P, Serag A, Hajnal J, Edwards A, Counsell S, Rueckert D. Automatic whole brain MRI segmentation of the developing neonatal brain. *IEEE Transactions on Medical Imaging*. 2014 Sep.33:1818–31. [PubMed: 24816548]
- Makropoulos A, Robinson EC, Schuh A, Wright R, Fitzgibbon S, Bozek J, Counsell SJ, Steinweg J, Passerat-Palmbach J, Lenz G, Mortari F, et al. The Developing Human Connectome Project: a minimal processing pipeline for neonatal cortical surface reconstruction. *Neuroimage*. 2018 Jun. 173:88–112. [PubMed: 29409960]
- Meng Y, Li G, Lin W, Gilmore JH, Shen D. Spatial distribution and longitudinal development of deep cortical sulcal landmarks in infants. *NeuroImage*. 2014 Oct.100:206–218. [PubMed: 24945660]
- Moeskops, P; Benders, MJNL; Pearlman, PC; Kersbergen, KJ; Leemans, A; Viergever, MA; Išgum, I. Assessment of quantitative cortical biomarkers in the developing brain of preterm infants. *SPIE Medical Imaging Computer-Aided Diagnosis*; 2013. 867011–867011-7.
- Moore J, Guan Y. Cytoarchitectural and axonal maturation in human auditory cortex. *Journal of the Association for Research in Otolaryngology*. 2001 Dec.2:297–311. [PubMed: 11833605]
- Robinson E, Garcia K, Glasser M, Chen Z, Coalson T, Makropoulos A, Bozek J, Wright R, Schuh A, Webster M, Hutter J, et al. Multimodal surface matching with higher-order smoothness constraints. *Neuroimage*. 2018 Feb.167:453–465. [PubMed: 29100940]
- Robinson E, Jbabdi S, Glasser M, Andersson J, Burgess G, Harms M, Smith S, Essen DV, Jenkinson MSM. MSM: a new flexible framework for Multimodal Surface Matching. *NeuroImage*. 2014 Oct. 100:414–426. [PubMed: 24939340]
- Robinson, EC; Glocker, B; Rajchl, M; Rueckert, D. Discrete optimisation for group-wise cortical surface atlasing. *The IEEE Conference on Computer Vision and Pattern Recognition (CVPR) Workshops*; 2016 Jun.
- Rueckert D, Sonoda L, Hayes C, Hill D, Leach M, Hawkes D. Nonrigid registration using free-form deformations: application to breast MR images. *IEEE Transactions on Medical Imaging*. 1999 Aug.18:712–721. [PubMed: 10534053]
- Rutherford, M. MRI of the Neonatal Brain. Saunders; London, England: 2002. URL visited on <http://www.mrineonatalbrain.com/index.php> [15November2016]
- Serag A, Aljabar P, Ball G, Counsell S, Boardman J, Rutherford M, Edwards A, Hajnal J, Rueckert D. Construction of a consistent high-definition spatio-temporal atlas of the developing brain using adaptive kernel regression. *NeuroImage*. 2012 Feb.59:2255–65. [PubMed: 21985910]
- Singh, N, Niethammer, M. *Splines for Diffeomorphic Image Regression*. Springer International Publishing; Cham: 2014. 121–129.
- Soun JE, Liu MZ, Cauley KA, Grinband J. Evaluation of neonatal brain myelination using the T1- and T2-weighted MRI ratio. *Journal of Magnetic Resonance Imaging*. 2016; doi: 10.1002/jmri.25570
- Toga AW, Thompson PM. Mapping brain asymmetry. *Nature Reviews Neuroscience*. 2003 Jan.4:37–48. [PubMed: 12511860]
- Van Essen D, Dierker D. Surface-based and probabilistic atlases of primate cerebral cortex. *Neuron*. 2007 Oct.56:209–225. [PubMed: 17964241]
- Van Essen D, Glasser M, Dierker D, Harwell J, Coalson T. Parcellations and hemispheric asymmetries of human cerebral cortex analyzed on surface-based atlases. *Cerebral Cortex*. 2012 Oct.22:2241–2262. [PubMed: 22047963]
- Van Essen DC. A population-average, landmark- and surface-based (pals) atlas of human cerebral cortex. *NeuroImage*. 2005; 28(3):635–662. [PubMed: 16172003]

- Wang Q, Kim M, Shi Y, Wu G, Shen D, Initiative ADN. Predict brain MR image registration via sparse learning of appearance and transformation. *Medical Image Analysis*. 2015 Feb.20:61–75. [PubMed: 25476412]
- Wright R, Makropoulos A, Kyriakopoulou V, Patkee P, Koch L, Rutherford M, Hajnal J, Rueckert D, Aljabar P. Construction of a fetal spatio-temporal cortical surface atlas from in utero MRI: Application of spectral surface matching. *NeuroImage*. 2015 Oct.120:467–480. [PubMed: 26070259]
- Yeo B, Sabuncu M, Vercauteren T, Ayache N, Fischl B, Golland P. Spherical demons: Fast diffeomorphic landmark-free surface registration. *IEEE Transactions on Medical Imaging*. 2010 Mar.29:650–668. [PubMed: 19709963]

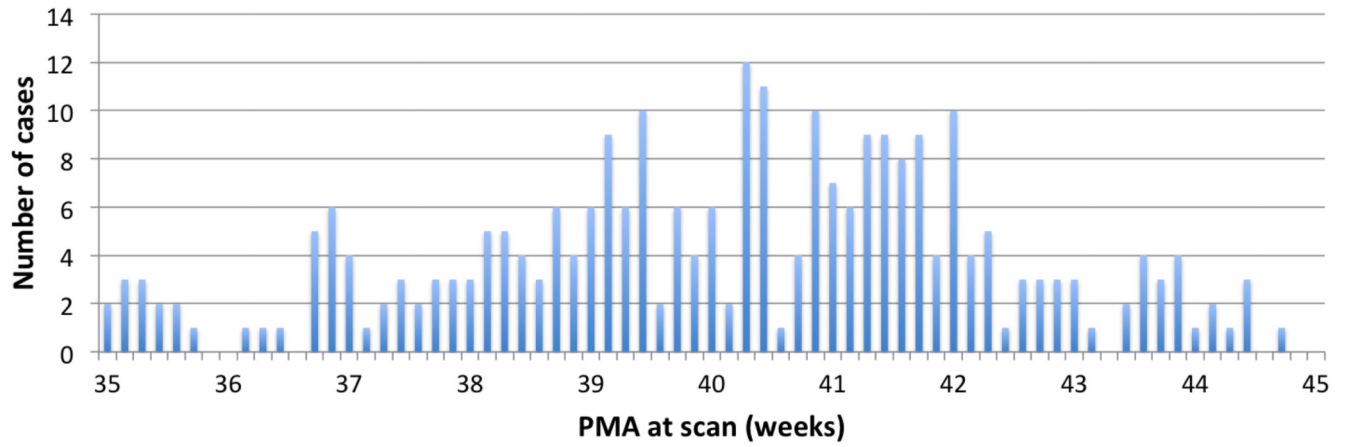


Figure 1.
Histogram of PMA at the time of scan.

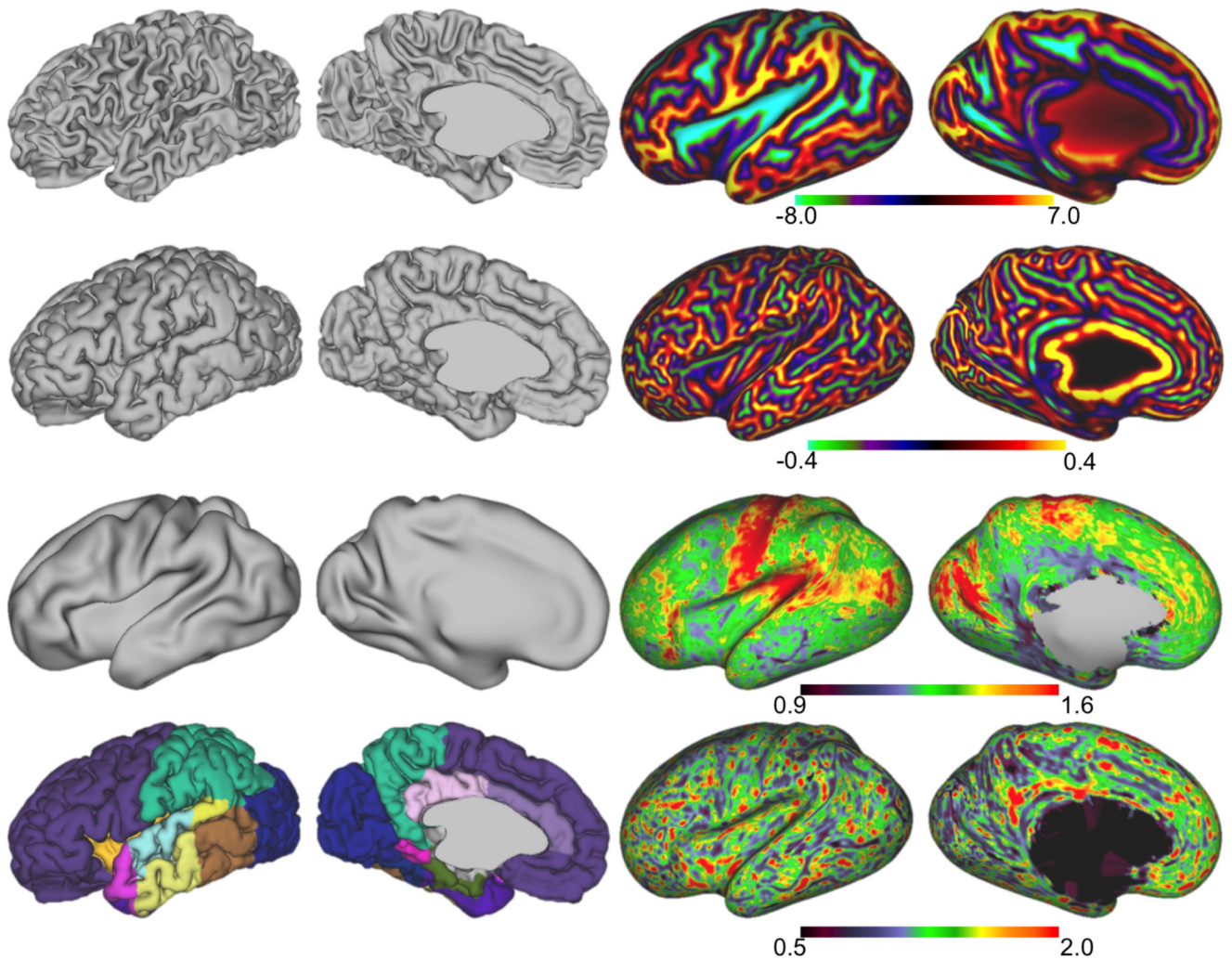


Figure 2. Exemplar surfaces and feature sets for an individual scanned at 40 weeks PMA (left hemisphere, medial and lateral views). Left from top to bottom: white matter surface, pial surface, inflated surface, cortical labels; right from top to bottom: sulcal depth map, mean curvature, T1w/T2w myelin maps, cortical thickness (all features shown on the very inflated surface).

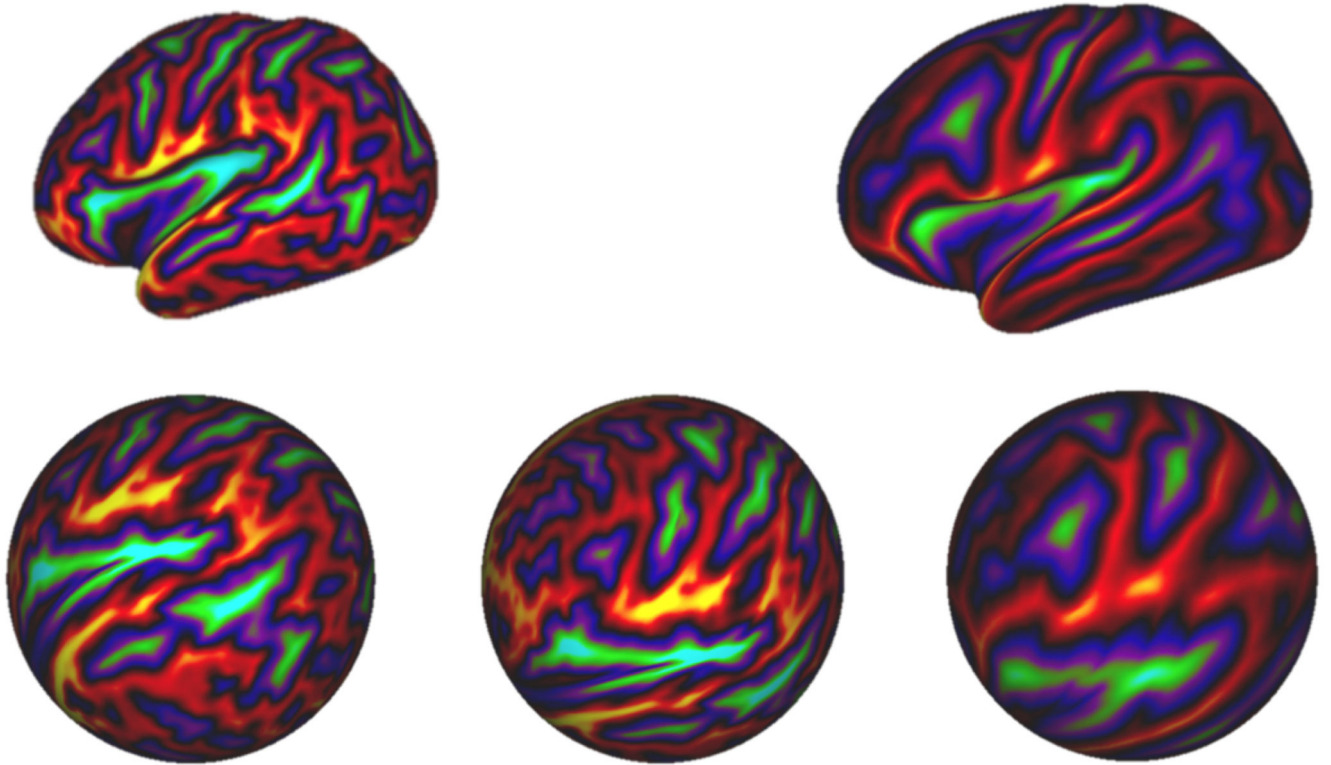


Figure 3.

Exemplar sulcal depth maps for: an individual projected on very inflated surface scanned at 40 weeks PMA (top left), and Conte69 atlas (top right) projected on very inflated surfaces (left hemisphere). Individual sphere (bottom left) rotates in reference to Conte69 sphere (bottom right) until the sulcal depth features align (bottom middle).

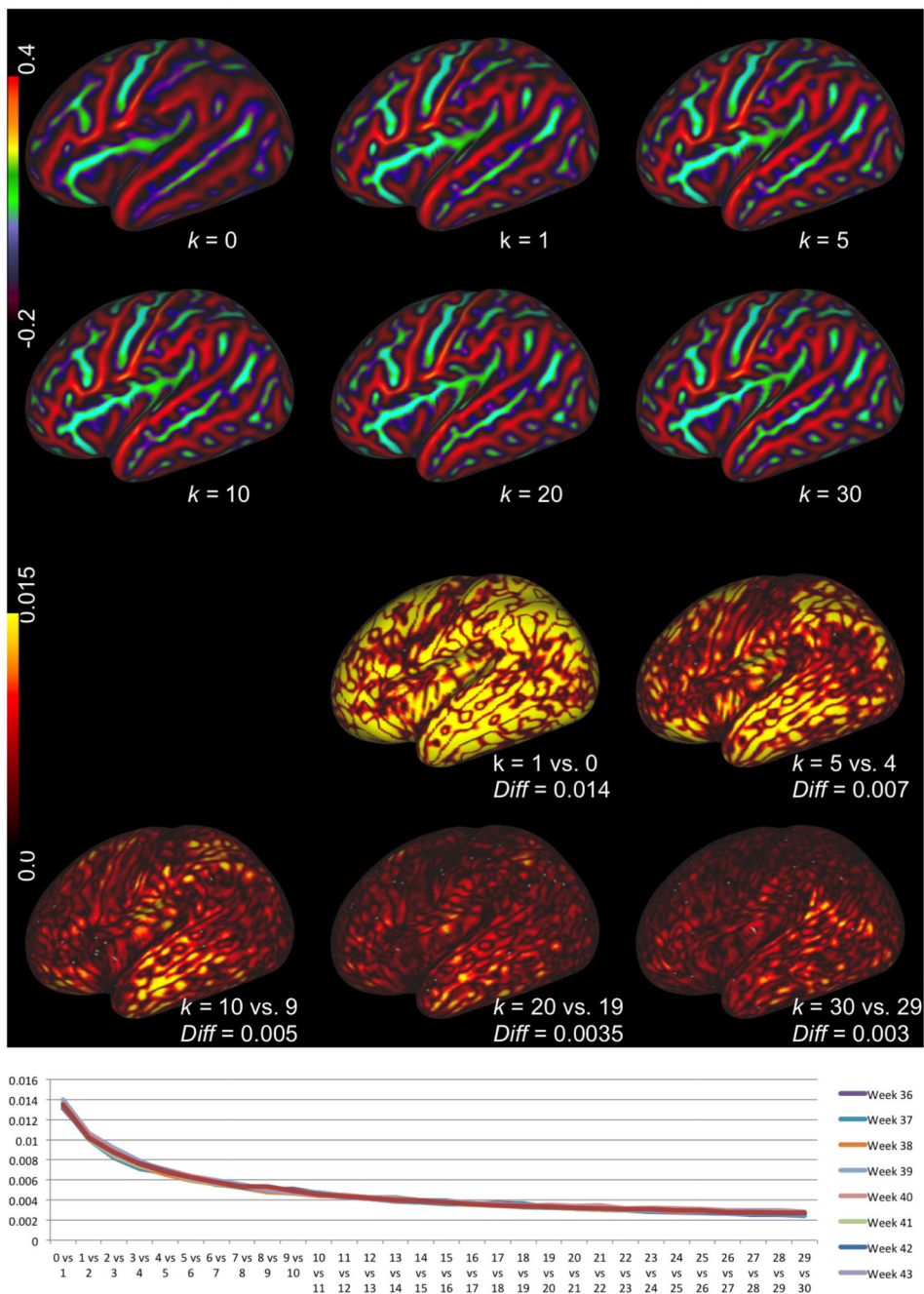


Figure 4. Curvature atlas for week 40 after initialisation ($k = 0$) and after different number of iterations ($k = 1, 5, 10, 20, 30$) (top rows). Map of vertex-wise difference of atlas curvature maps between iterations k and $k - 1$ (middle rows), where *Diff* represents mean across the brain of absolute vertex-wise difference. (left hemisphere, projected on the very inflated surface). Bottom: plot of mean across the brain of absolute vertex-wise difference.

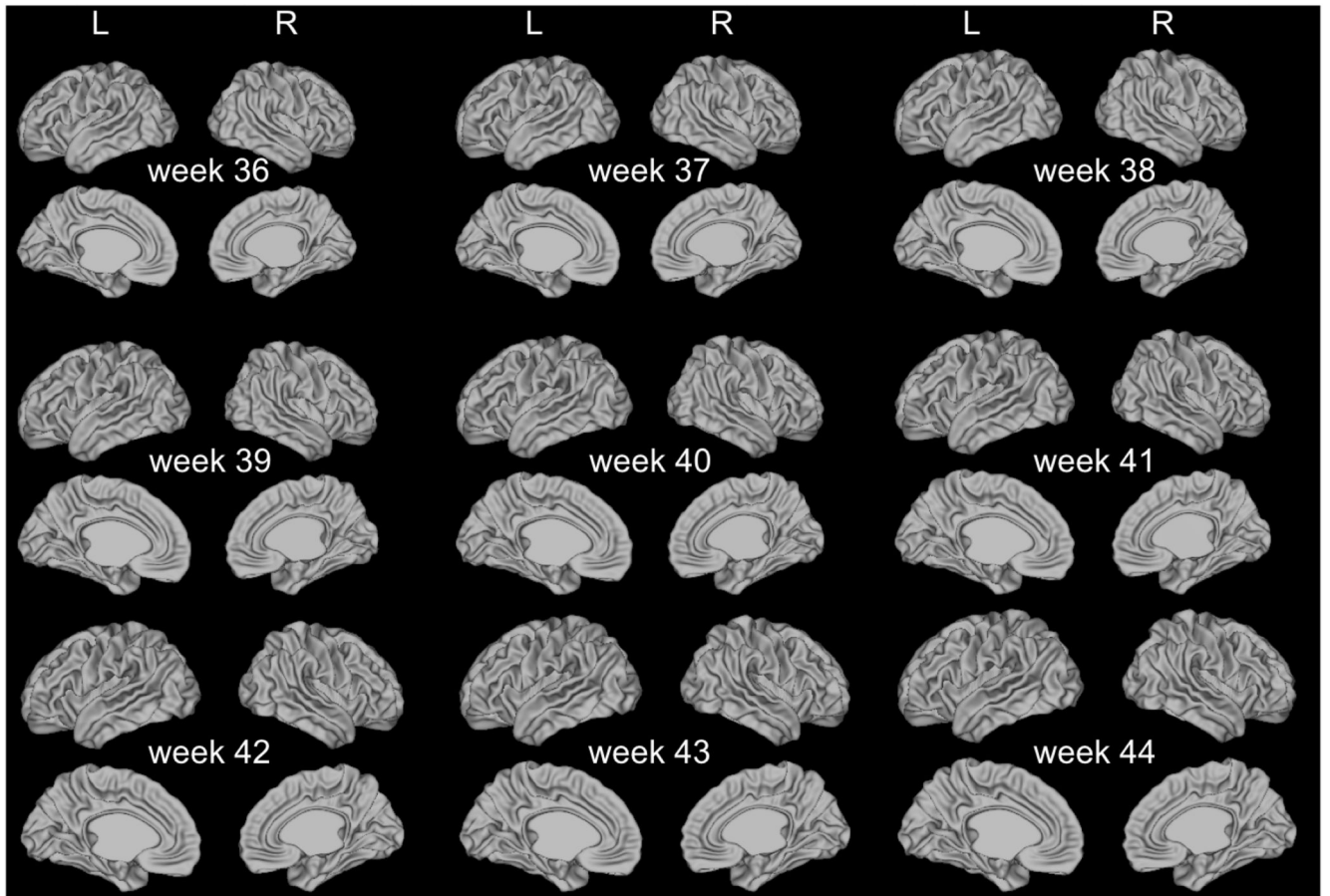


Figure 5. Final anatomical cortical white matter surface atlas spanning 36 to 44 weeks (left and right hemispheres).

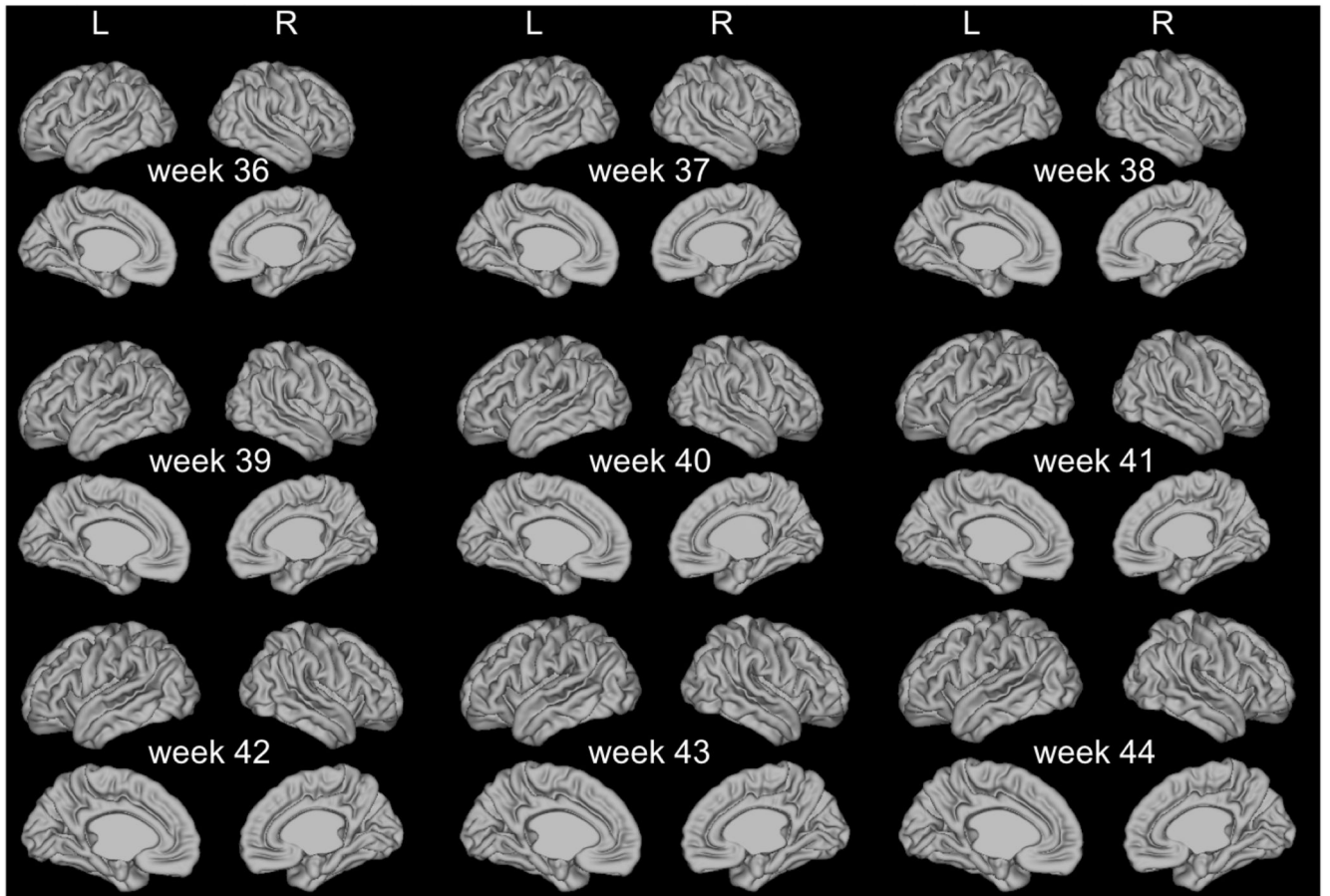


Figure 6. Final anatomical cortical pial surface atlas spanning 36 to 44 weeks (left and right hemispheres, lateral and medial views).

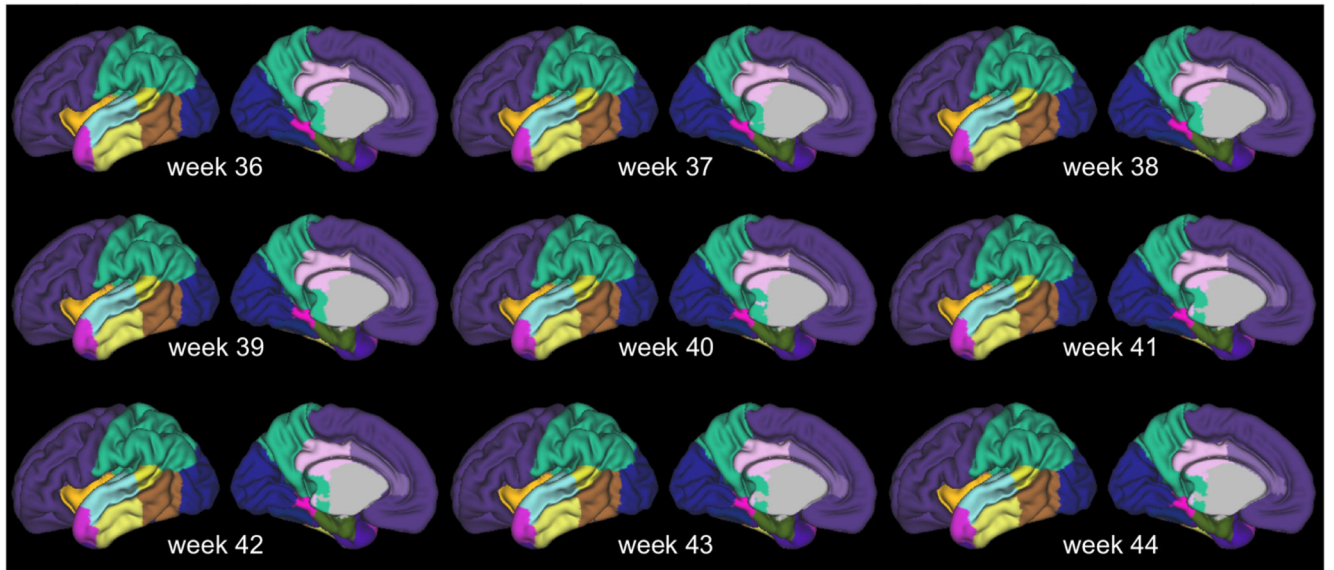


Figure 7. Cortical label atlas (maximum probability version) spanning 36 to 44 weeks on the final template (left hemisphere, lateral and medial views).

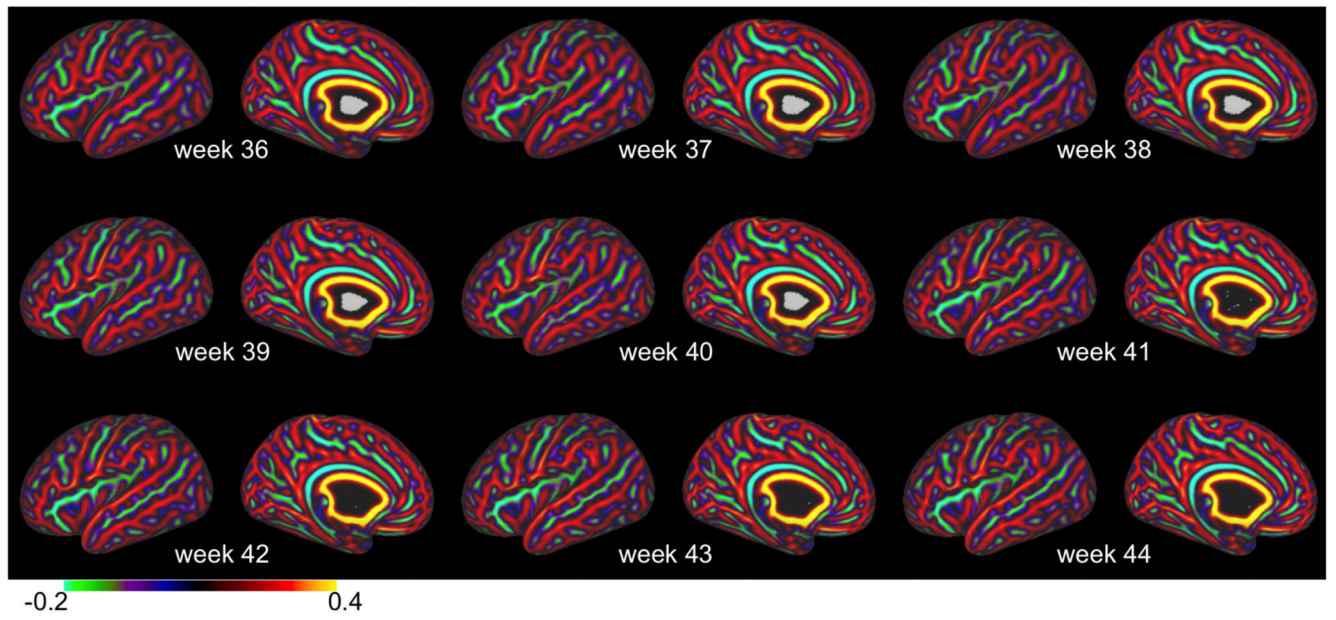


Figure 8.

Mean curvature atlas spanning 36 to 44 weeks on the final template (data projected on the very inflated surface, left hemisphere, lateral and medial views).

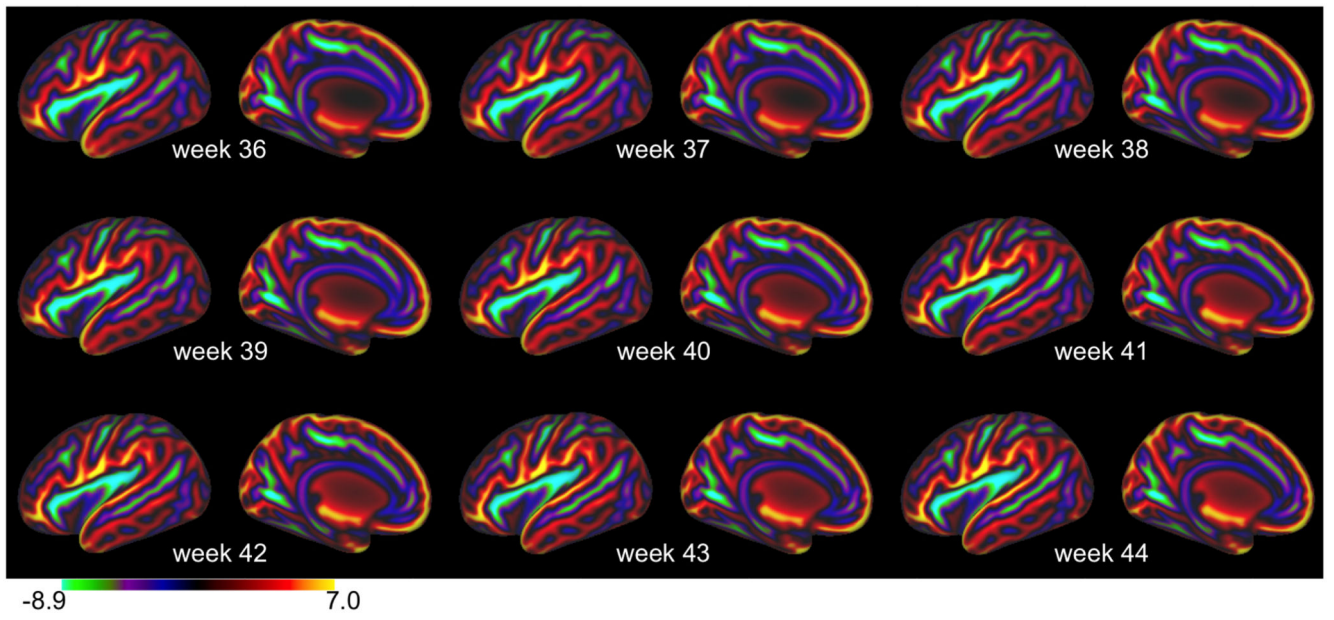


Figure 9. Sulcal depth map atlas spanning 36 to 44 weeks on the final template (data projected on the very inflated surface, left hemisphere, lateral and medial views).

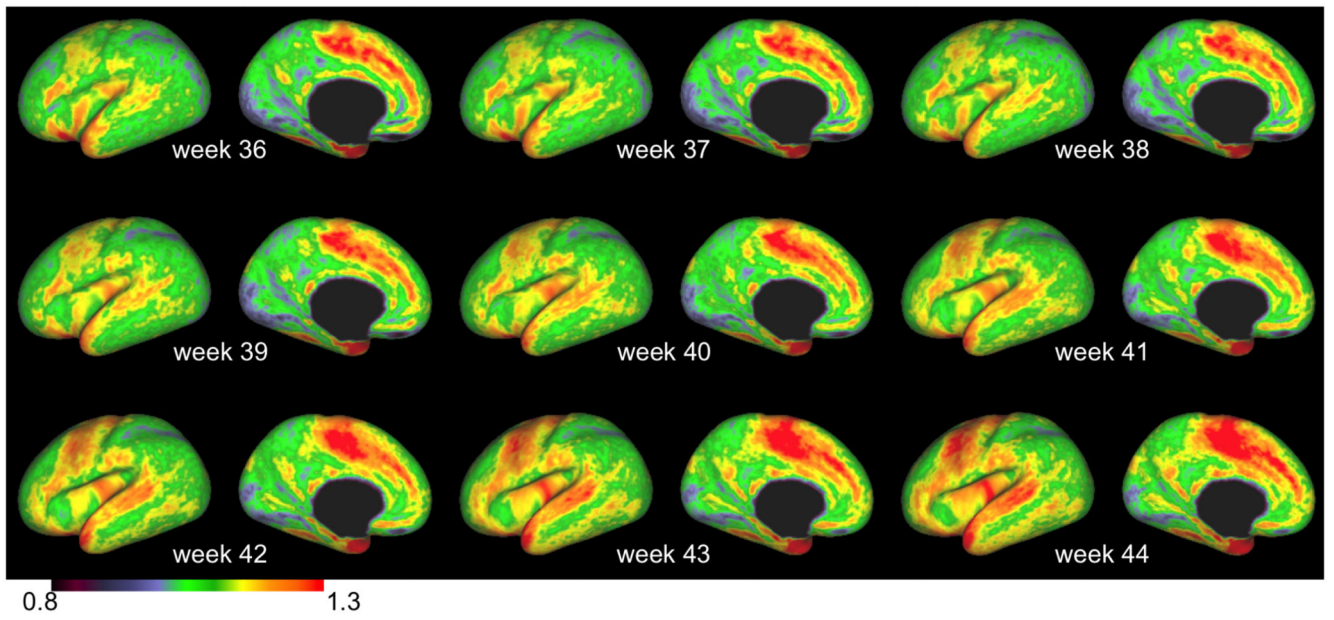


Figure 10. Thickness atlas spanning 36 to 44 weeks on the final template (data projected on the very inflated surface, left hemisphere, lateral and medial views).

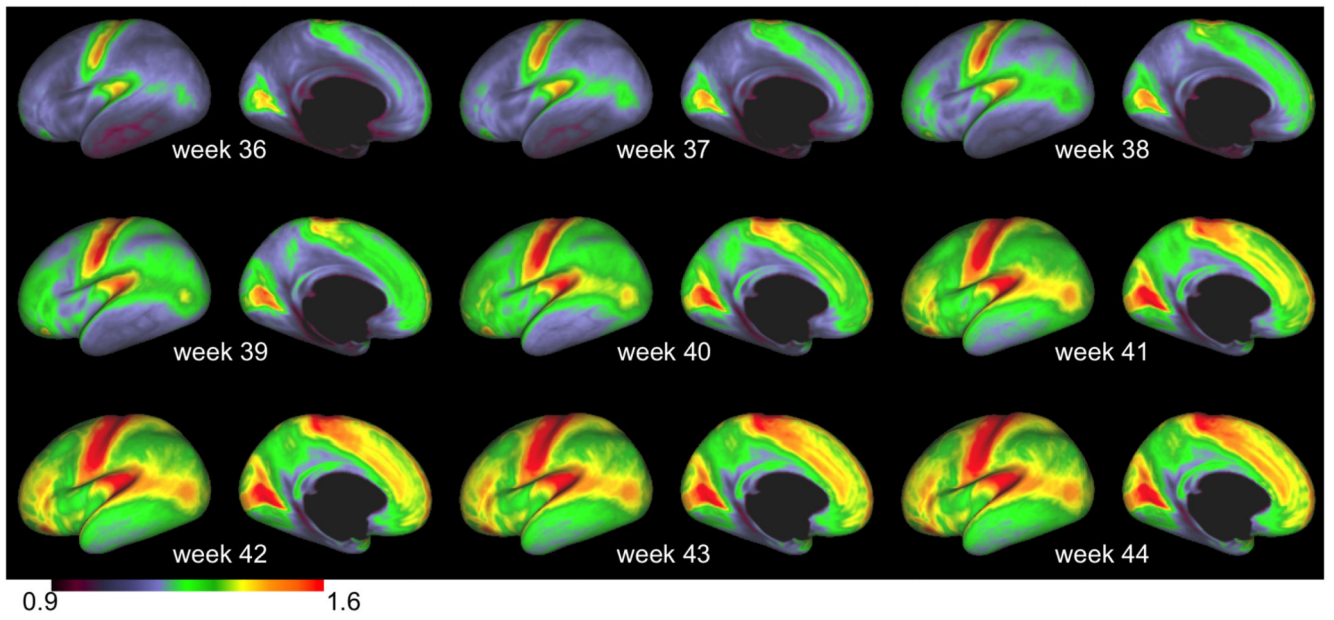


Figure 11. T1w/T2w myelin atlas spanning 36 to 44 weeks on the final template (data projected on the very inflated surface, left hemisphere, lateral and medial views).

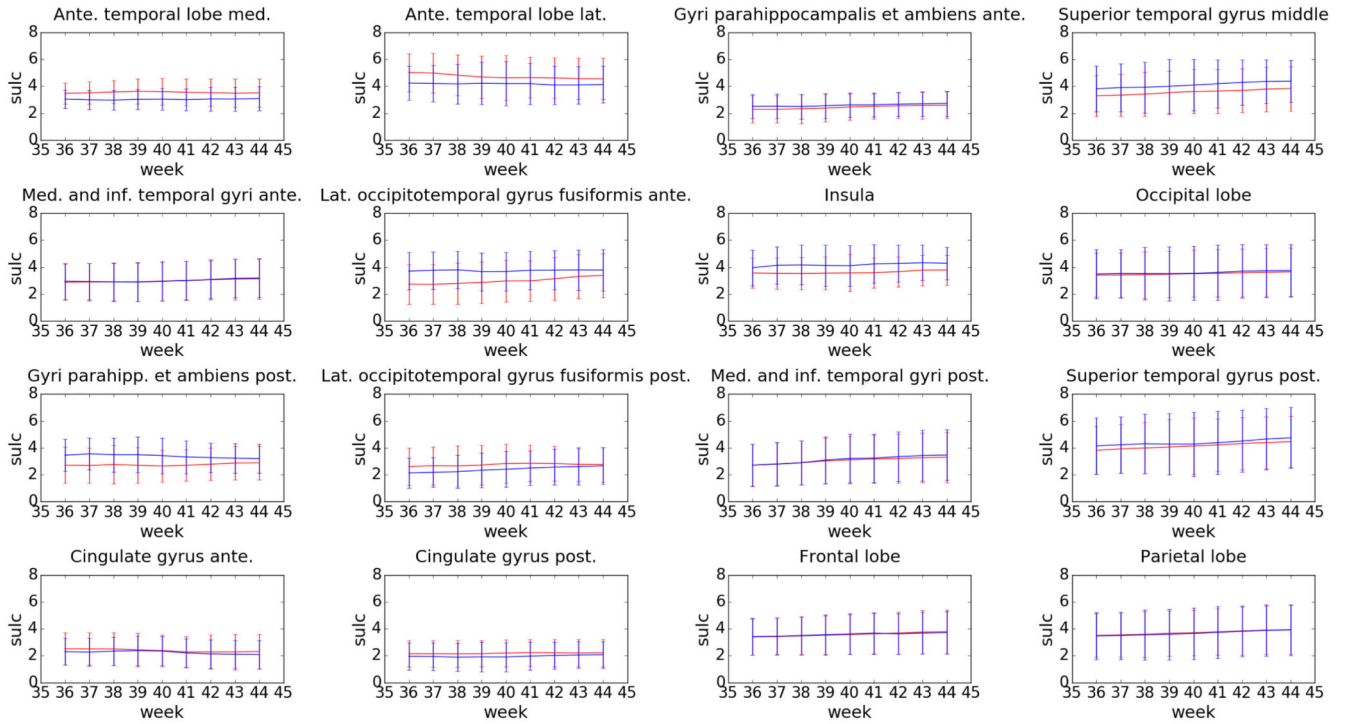


Figure 12. Weighted average across subjects of absolute sulcal depth values per cortical region (red line - left hemisphere, blue line - right hemisphere; lat.=lateral, med.=medial, ante.=anterior, post.=posterior, inf.=inferior). Error bars represent weighted standard deviation across subjects.

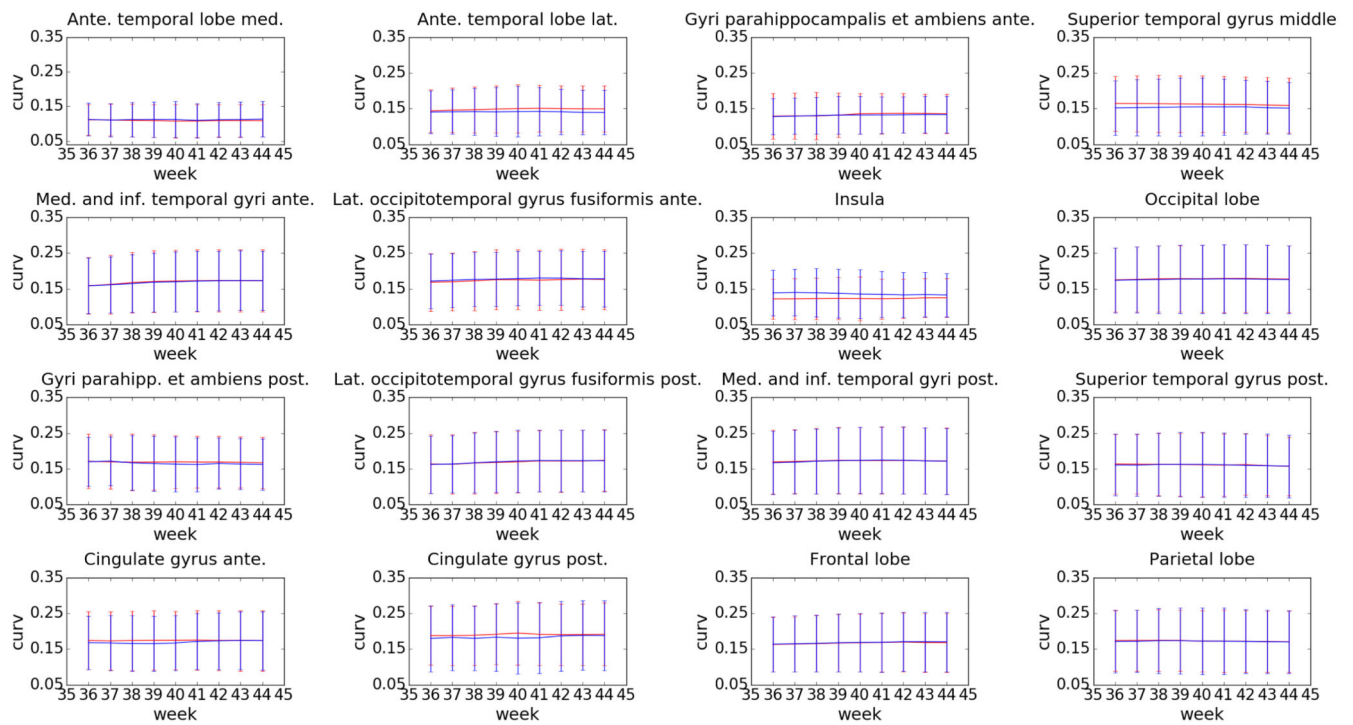


Figure 13.

Weighted average across subjects of absolute curvature values per cortical region (red line - left hemisphere, blue line - right hemisphere; lat.=lateral, med.=medial, ante.=anterior, post.=posterior, inf.=inferior). Error bars represent weighted standard deviation across subjects.

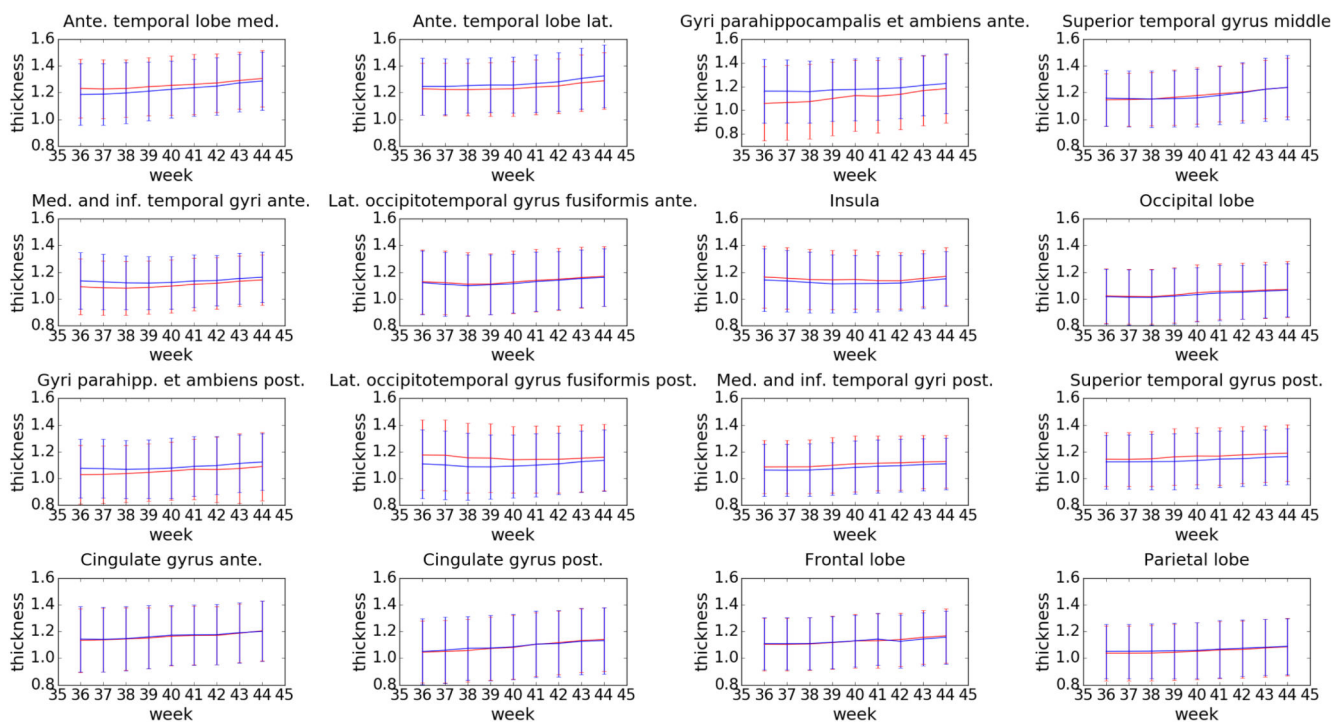


Figure 14. Weighted average across subjects of thickness values per cortical region (red line - left hemisphere, blue line - right hemisphere; lat.=lateral, med.=medial, ante.=anterior, post.=posterior, inf.=inferior). Error bars represent weighted standard deviation across subjects.

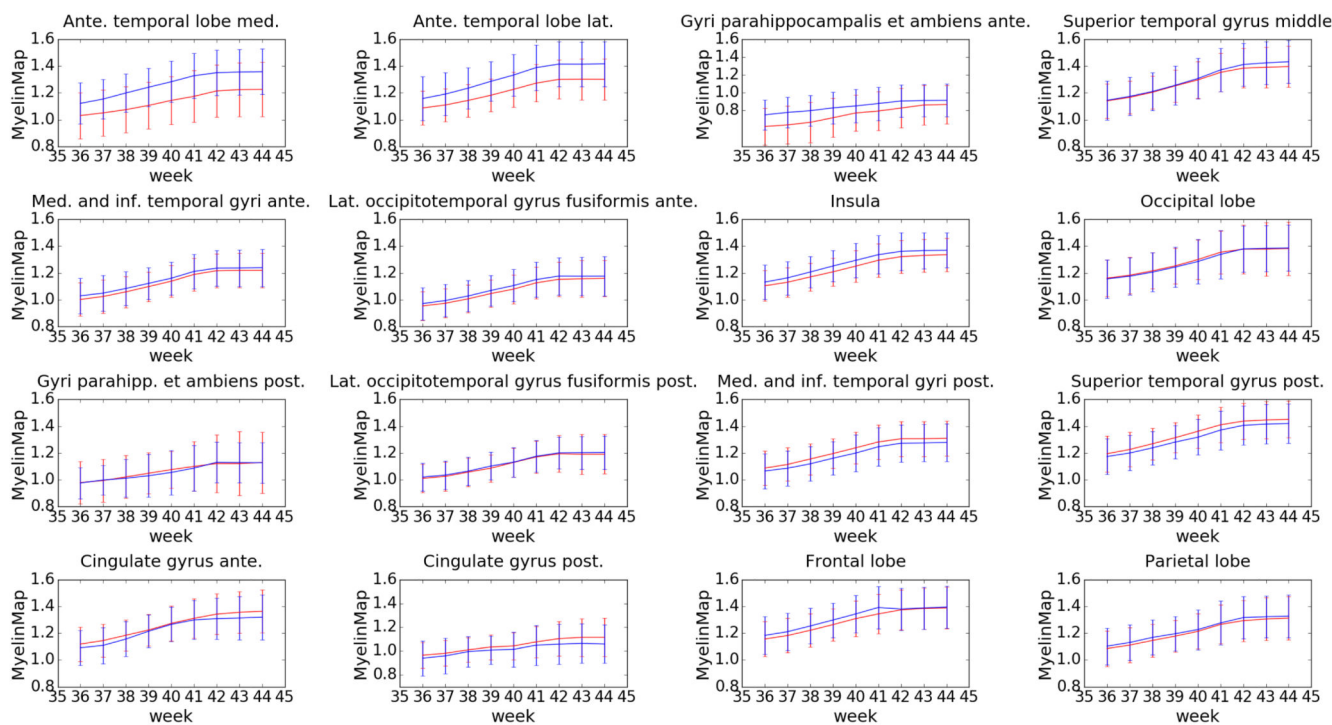
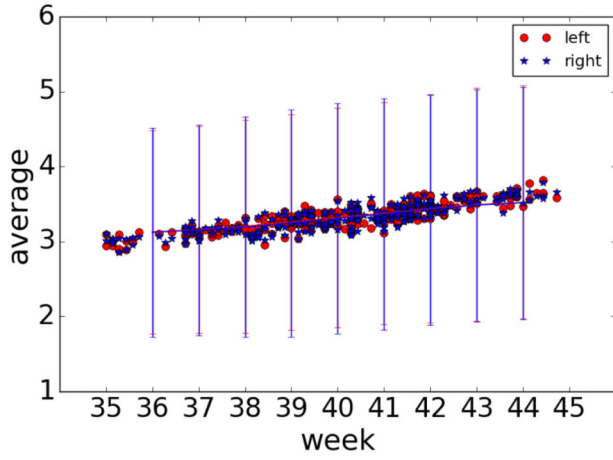
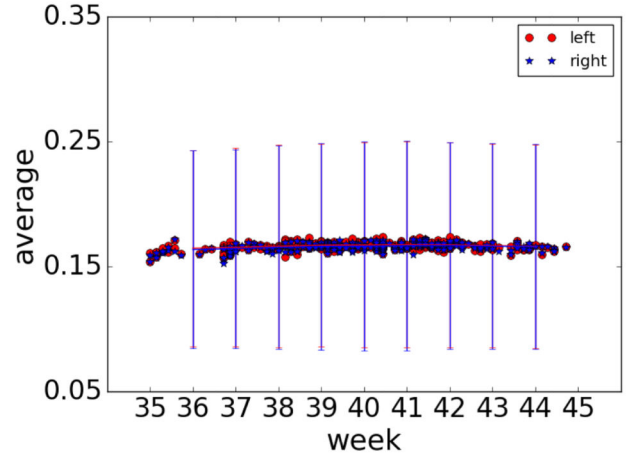


Figure 15.

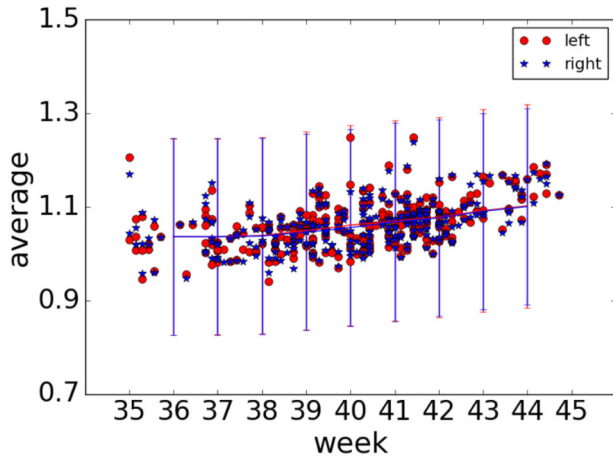
Weighted average across subjects of T1w/T2w myelin map values per cortical region (red line - left hemisphere, blue line - right hemisphere; lat.=lateral, med.=medial, ante.=anterior, post.=posterior, inf.=inferior). Error bars represent weighted standard deviation across subjects.



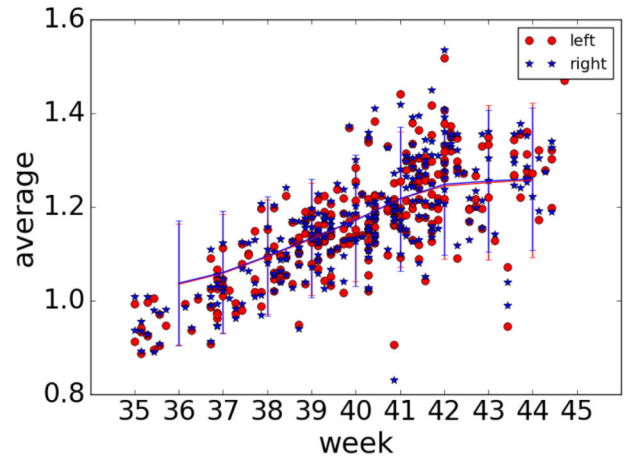
(a) Sulcal depth



(b) Curvature



(c) Thickness



(d) T1w/T2w myelin

Figure 16.

Mean of absolute feature map values across the whole brain for individual subjects spanning 36 to 44 weeks (red dots - left hemisphere, blue stars - right hemisphere) and weighted average across subjects of feature map values across the whole brain with error bars representing weighted standard deviation across subjects (red line - left hemisphere, blue line - right hemisphere).

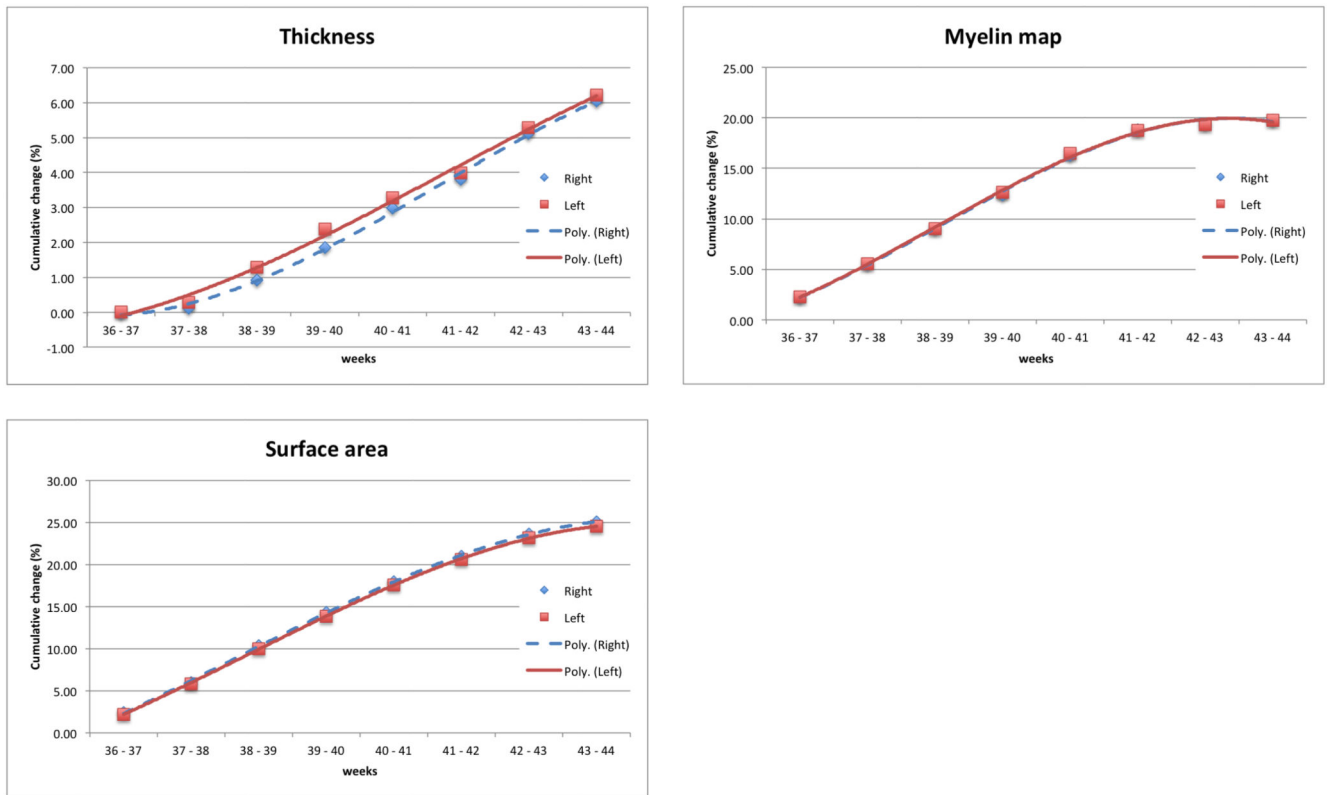


Figure 17. Cumulative sum of percent change of thickness, T1w/T2w myelin maps and surface area between weeks for left (red dots and fitted lines) and right (blue dots and fitted lines) hemispheres.

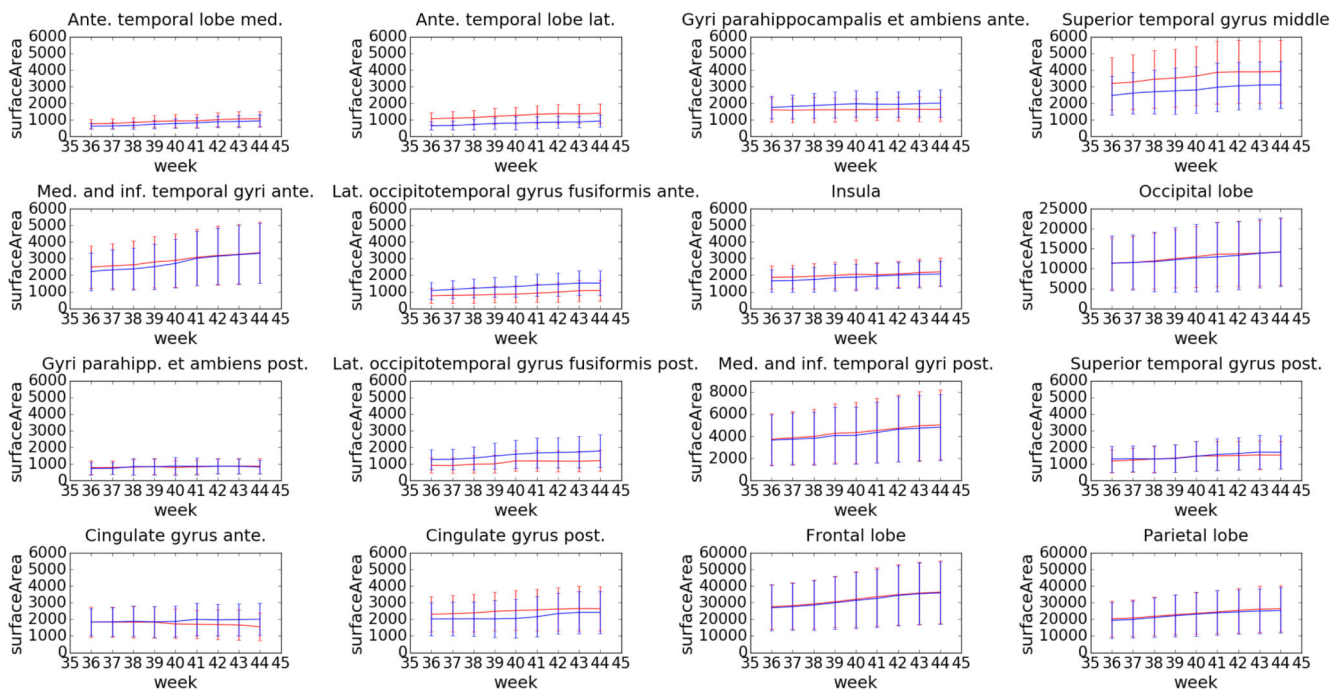


Figure 18. Weighted average across subjects of surface area values per cortical region (red line - left hemisphere, blue line - right hemisphere; lat.=lateral, med.=medial, ante.=anterior, post.=posterior, inf.=inferior). Error bars represent weighted standard deviation across subjects.

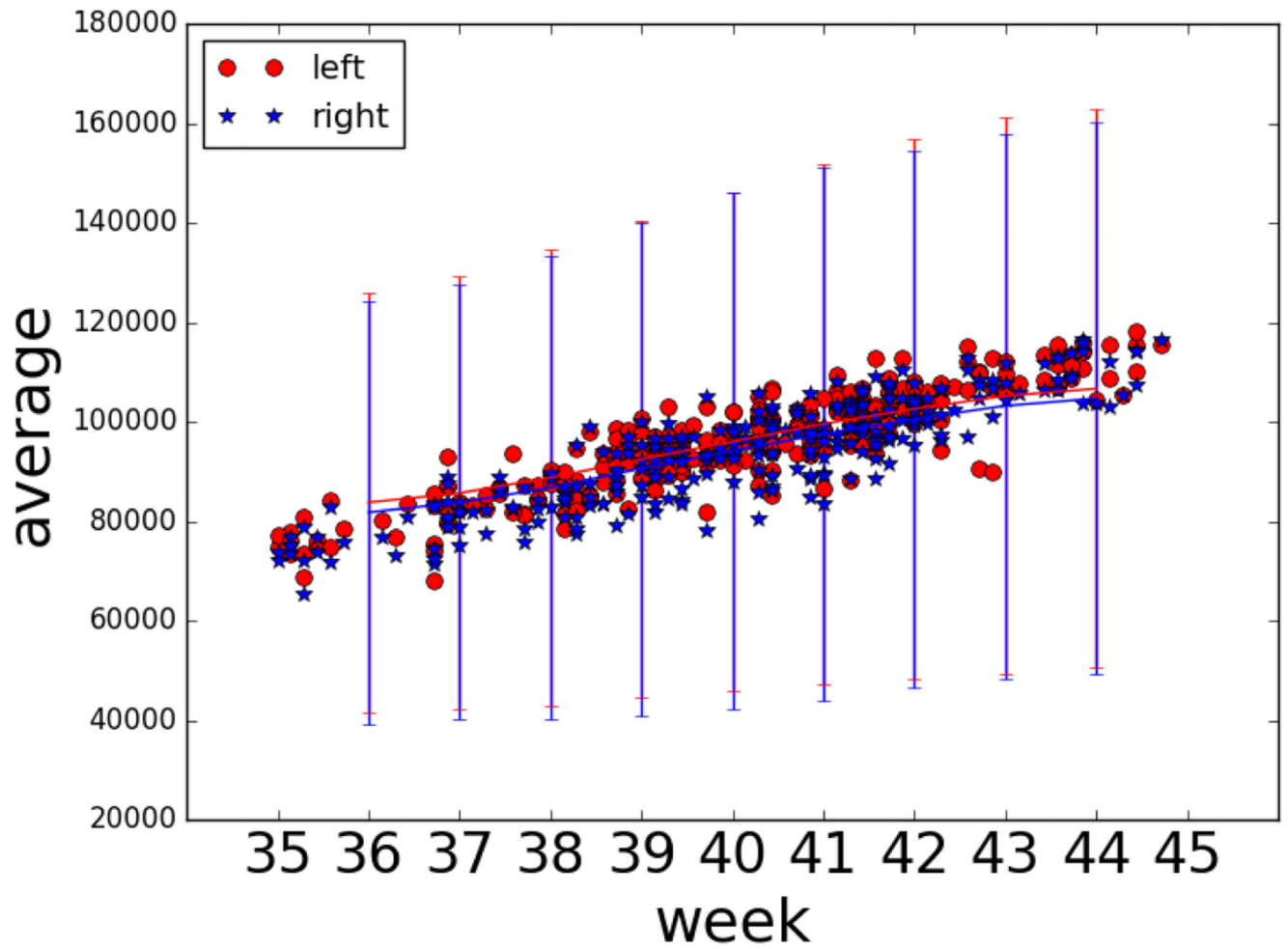


Figure 19.

Mean of surface area across the whole brain for individual subjects spanning 36 to 44 weeks (red dots - left hemisphere, blue stars - right hemisphere) and weighted average across subjects of surface area across the whole brain with error bars representing weighted standard deviation across subjects (red line - left hemisphere, blue line - right hemisphere).

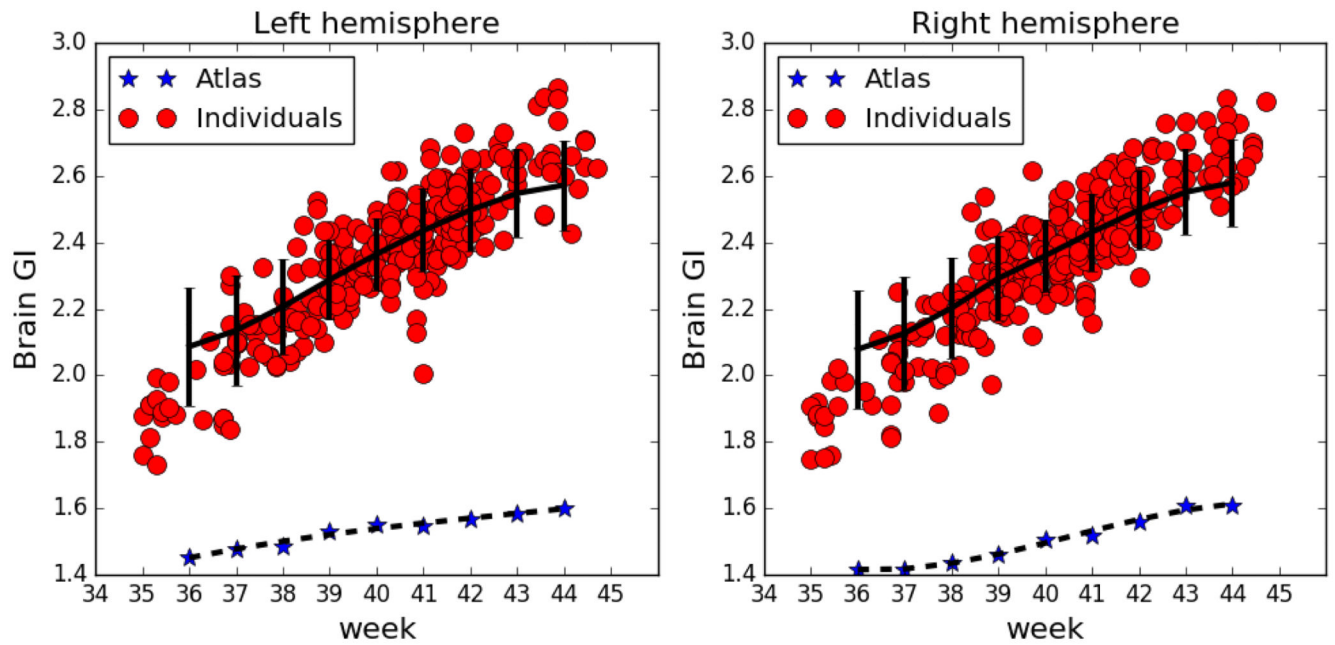


Figure 20.

Gyrification index (GI) for left and right hemisphere for individual subjects (red dots), with weighted average across subjects and error bars representing weighted standard deviation across subjects (black line), and for the final anatomical cortical pial surface atlas (blue stars and dashed line), spanning 36 to 44 weeks.

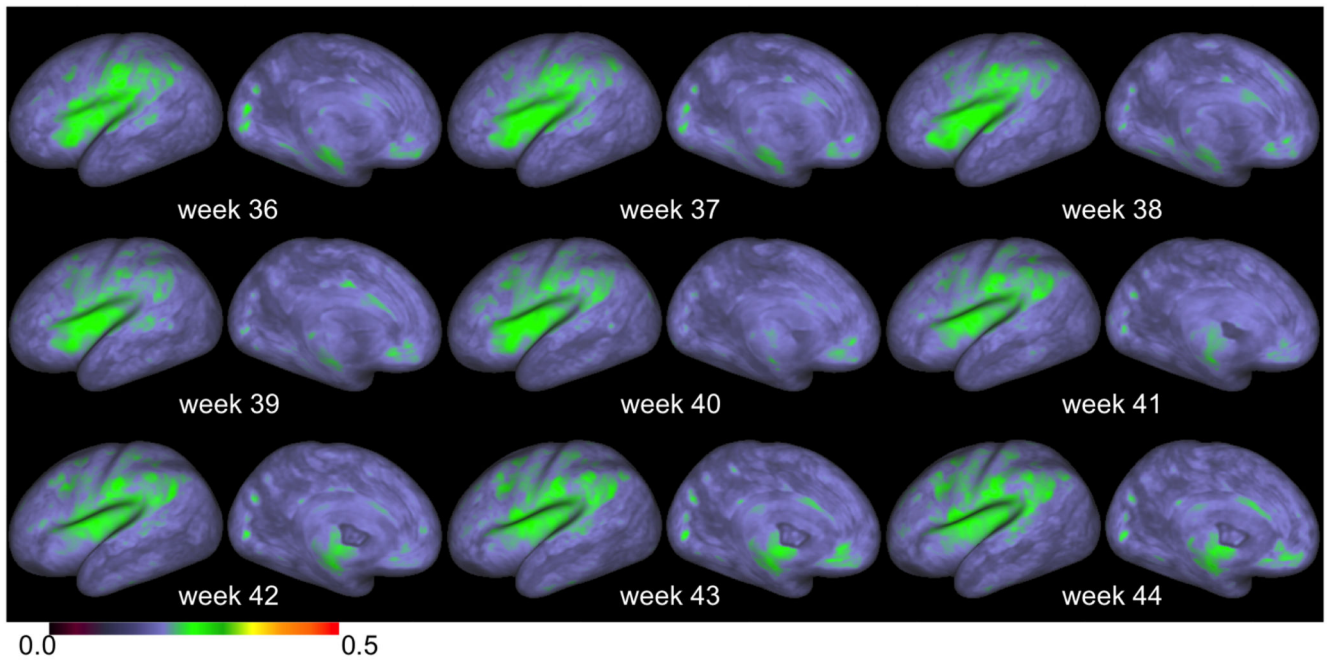


Figure 21.

Average across subjects of the absolute areal distortion map, spanning 36 to 44 weeks (data projected on the inflated surface, left hemisphere, lateral and medial views).

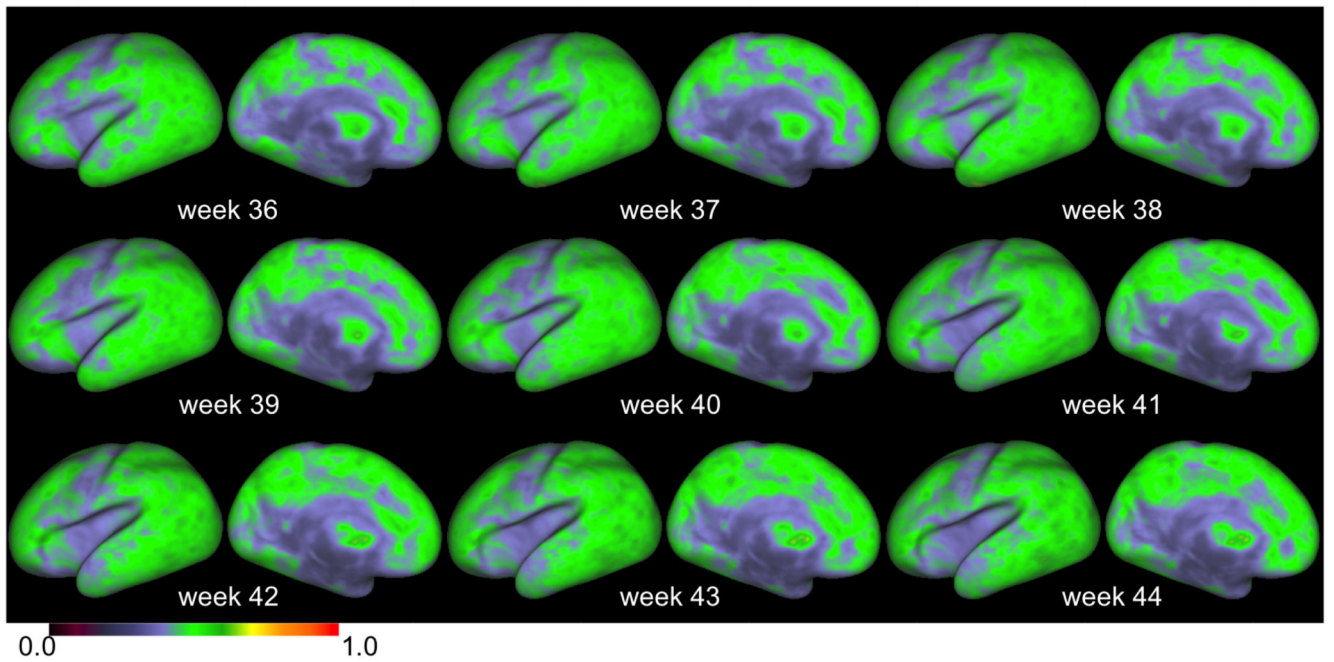


Figure 22.

Average across subjects of the anisotropic deformation map, spanning 36 to 44 weeks (data projected on the inflated surface, left hemisphere, lateral and medial views).

Table 1
Maximum and minimum across subjects of the areal distortion and maximum of the anisotropic deformation spanning 36 to 44 weeks for left and right hemispheres.

Week	Areal				Anisotropic	
	Max		Min		Max	
	L	R	L	R	L	R
36	0.61	0.65	-0.42	-0.42	1.28	1.17
37	0.62	0.65	-0.42	-0.41	1.19	1.22
38	0.64	0.62	-0.42	-0.41	1.21	1.27
39	0.66	0.64	-0.43	-0.42	1.20	1.98
40	0.68	0.61	-0.42	-0.42	1.25	1.47
41	0.65	0.68	-0.43	-0.42	2.20	1.28
42	0.64	0.63	-0.42	-0.41	2.04	1.20
43	0.68	0.63	-0.43	-0.42	2.06	1.19
44	0.66	0.66	-0.42	-0.41	2.18	1.20

Table 2
Mean and maximum across subjects of the areal distortion and anisotropic deformation across 36 to 44 weeks and both hemispheres.

Areal distortion		Anisotropic distortion	
Mean	Max	Mean	Max
0.17	0.68	0.46	2.2